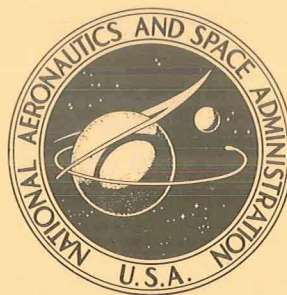# NASA TECHNICAL NOTE

NASA TN D-7611

NASA TN D-7611

CASE FILE COPY

PRELIMINARY STUDY OF A POSSIBLE AUTOMATIC LANDING SYSTEM

by Windsor L. Sherman and Sylvia W. Winfrey

Langley Research Center
Hampton, Va. 23665

AMERICAN REVOLUTION BICENTENNIAL 1776-1976

NATIONAL AERONAUTICS AND SPACE ADMINISTRATION • WASHINGTON, D. C. • JULY 1974

1. Report No. NASA TN D-7611	2. Government Accession No.	3. Recipient's Catalog No.
4. Title and Subtitle PRELIMINARY STUDY OF A POSSIBLE AUTOMATIC LANDING SYSTEM		5. Report Date July 1974
		6. Performing Organization Code
7. Author(s) Windsor L. Sherman and Sylvia W. Winfrey		8. Performing Organization Report No. L-9246
		10. Work Unit No. 768-81-02-01
9. Performing Organization Name and Address NASA Langley Research Center Hampton, Va. 23665		11. Contract or Grant No.
		13. Type of Report and Period Covered Technical Note
12. Sponsoring Agency Name and Address National Aeronautics and Space Administration Washington, D.C. 20546		14. Sponsoring Agency Code

15. Supplementary Notes

16. Abstract

Navigation and control laws for a possible automatic landing system have been investigated. The system makes use of data from an inertial table and either an airborne or ground radar to generate signals that guide the airplane to a landing. All landing maneuvers take place within a zone that extends 6000 m out from the touchdown point, 4000 m on each side of the runway center line, and 540 m high. The results show that the system can adequately control the airplane on steep, curved decelerating approaches to a landing that takes place with small errors from the desired landing point and desired airplane attitude. The system studied would interface well with the scanning beam microwave landing system (MLS). The use of this system with the MLS makes it possible to incorporate an independent landing monitor.

17. Key Words (Suggested by Author(s)) Guidance Terminal area Landing	18. Distribution Statement Unclassified — Unlimited STAR Category 21		
19. Security Classif. (of this report) Unclassified	20. Security Classif. (of this page) Unclassified	21. No. of Pages 66	22. Price* $3.75

PRELIMINARY STUDY OF A POSSIBLE

AUTOMATIC LANDING SYSTEM

By Windsor L. Sherman and Sylvia W. Winfrey
Langley Research Center

SUMMARY

Navigation and control laws for a possible automatic landing system have been investigated. The system makes use of data from an inertial table and either an airborne or ground radar to generate signals that guide the airplane to a landing. All landing maneuvers take place within a zone that extends 6000 m out from the touchdown point, 4000 m on each side of the runway center line, and 540 m high. The results show that the system can adequately control the airplane on steep, curved decelerating approaches to a landing that takes place with small errors from the desired landing point and desired airplane attitude. The system studied would interface well with the scanning beam microwave landing system (MLS). The use of this system with the MLS makes it possible to incorporate an independent landing monitor.

INTRODUCTION

The approach and landing phase of flight operations is one of the more hazardous portions of aircraft flight with approximately 50 percent of the accidents occurring during this phase. Inclement weather not only increases the hazards of approach and landing but decreases the efficiency of air transportation by delays resulting from waiting stacks and required use of distant alternate airports. A reliable and efficient automatic landing system that reduces pilot workload during the approach and landing and the effects of inclement weather would increase the safety and efficiency of air transportation. Military aircraft operations would derive similar benefits from such a system.

Automatic landing systems are not a new idea; several have been developed for current transport aircraft, but their use in day-to-day operations has been minimal. These automatic landing systems, references 1 and 2, are designed to work with the present instrument landing system (ILS). The basic mode of operation is riding the ILS beam to a landing. These systems are characterized by long, straight approaches and shallow

glide slopes. This type of operation subjects the airplane to possible undesirable external disturbances over long periods of time when it lacks maneuver room. In addition, ILS beams on which this system depends are subject to distortions from weather conditions and over-flights by aircraft. The ILS mode of landing an aircraft also imposes an objectionable noise footprint on communities around the airport.

A study of recent developments in airborne radar such as the phased array antenna and of the scanning beam microwave landing system (MLS), references 3 and 4, indicated that the tools were at hand for the development of a total airborne automatic landing system. This system should be capable of executing steep, curved approaches where the airplane would be under positive maneuver control at all times, shortening the time to land and reducing the exposure of nearby communities to objectionable noise. Several investigations of such an automatic landing system have already been made. The favorable results incorporated in reference 5 reinforced the concept of the use of airborne radar in automatic landing systems. Reference 6 presents methods for navigation in the terminal area and reference 7 discusses a feed forward automatic landing system for use with the MLS. The system described in reference 7 can use the MLS information to guide the airplane along steep, curved approaches which are defined by a model trajectory generator.

The automatic-landing-system concept reported herein is a feedback type system and the airplane flies a space curve that is dependent on the heading error with respect to the runway and its position with respect to the runway center line. The system uses airborne digital computers to process the information obtained from an inertial measuring unit (IMU) and either an airborne radar with runway enhancement or a scanning beam MLS into commands that control the state of the airplane and effect a landing. Digital computers were assumed because this type of computer is more adaptable to the complicated logic required by the autoland system. When the airborne radar is used in conjunction with the MLS, it is possible to provide an independent landing monitor which is an FAA (Federal Aviation Administration) requirement (ref. 8) for automatic landing systems.

The study reported herein concentrated on the investigation of the control laws and logic required to control the airplane along steep, curved decelerating landing trajectories. As the airplane characteristics are not explicit in the control laws, these laws should be adaptable to different airplanes without major change. The system should be applicable to both civil and military aircraft operations. However, maneuver constraints dictated by passenger comfort indicated that civil operation would put a greater tax on the system capability; civil operations were therefore used as a base of the study.

The results are presented in the form of plots for ground and altitude tracks and tables of initial and touchdown conditions. Because winds, turbulence, and instrument noise were not considered in the study, the results are considered preliminary in nature.

SYMBOLS

The International System of Units is used throughout this report. All angles are in radians.

b   wing span

C_D drag coefficient

C_L lift coefficient

C_l rolling-moment coefficient

C_m pitching-moment coefficient

C_n yawing-moment coefficient

C_Y side-force coefficient

$\bar{c}$ mean aerodynamic chord

E   total error

g   acceleration of gravity

H   altitude

I_{y_1} moment of inertia about y_1-axis

I_{y_2} moment of inertia about y_2-axis

I_{y_3} moment of inertia about y_3-axis

m   mass

p   airplane roll rate about airplane axis

q   airplane pitch rate about airplane axis

R   radar range

$\vec{R}$ radar range vector

$\vec{R}_H$ two component range vector in z_j coordinates

$\vec{R}_{RTD}$ two component vectors from reflector to landing gate in z_j coordinates

r   airplane yaw rate about airplane axis

S   wing area

T   thrust

ΔT change in thrust

$\vec{\dot{T}}$ turning-rate vector

t   time

u   airplane speed along y_1-axis

V   airplane speed

$\vec{V}$ airplane velocity vector

V_T airplane velocity vector, magnitude

v   airplane speed along y_2-axis

w   airplane speed along y_3-axis

x_j radar coordinates

y_j airplane coordinates, referred to principal body axes

z_j quasi inertial coordinates

α angle of attack

β angle of sideslip

4

γ	flight-path angle
δ_a	aileron deflection angle
δ_e	elevator deflection angle
δ_f	flap deflection angle
δ_H	stabilizer deflection angle
δ_r	rudder deflection angle
δ_{sp}	spoiler deflection angle
ζ_j	runway coordinates, referred to desired landing point
η_j	inertial coordinates, translate with airplane
θ	Euler pitch angle
θ_a	radar azimuth angle
θ_{AA}	radar azimuth angle in z_j coordinates
θ_{AC}	command radar azimuth angle in z_j coordinates
θ_{AG}	azimuth angle for ground radar
θ_e	radar elevation angle
θ_{EE}	ground radar elevation angle in z_j coordinates
θ_{EG}	elevation angle for ground radar
τ	servo time constant
ϕ	Euler roll angle
ψ	Euler heading angle

Gains:

k_1 variable gain

k_2 variable gain

$k_3 = 0.8$

$k_4 = 3.0$ or 4.8

$k_5 = 5.0$

k_6 variable gain

$k_7 = 5.8$

$k_8 = 4.4$

$k_9 = 0.3$

$k_{10} = 7.7$

$k_{11} = 0.3$

$k_{12} = 1.1$

$k_{13} = 10.0$

$k_{14} = 1.0$ or 1.5

Subscripts:

c   command

E   error

i   initial

j   coordinate index, $j = 1, 2, 3$

ℓ limit

max   maximum

min   minimum

o   output

r   runway

A dot over a variable indicates differentiation with respect to time.

THE AUTOMATIC LANDING SYSTEM

A block diagram of the automatic-landing-system concept that was studied with the major system components and feedback paths is shown in figure 1. The system uses information obtained from an airborne radar or the scanning beam microwave landing system (MLS) and an inertial measuring unit (IMU) to guide the airplane from a point in space in the vicinity of the airport along a curved descending trajectory to a landing. While executing this trajectory, the speed of the airplane is changed from approach speed to landing speed. The block diagram shows both the airborne and ground radar of the MLS. When the MLS is used, the necessary data are transmitted to the airplane where they are processed according to the methods of appendix A before entering the system through the coordinate transformation block of figure 1. This dual radar capability can be used to provide the system with an independent landing monitor (ILM). The ILM would be implemented by using both airborne and ground radars and calculating the guidance commands in parallel computers, using the same algorithm. Comparison of the two sets of guidance commands would indicate whether the system is functioning properly.

The Radar and Inertial Measuring Unit

The equations used to represent the radar and IMU are given in appendix B. The form of the equations was selected so that radar and instrument noise could be added with ease at a later date. The radar equations are for the airborne radar but can be used to represent the ground radar as well. The airborne radar was selected because of the view angle constraint this type of radar imposes on the system. Generally speaking, the field of view of an airborne radar is restricted to cone about the center line of the airplane with a semiapex angle of 1.13446 rad. This restriction is critical in azimuth. However, recent developments in airborne radar have increased the azimuth look angle to about $\pm\frac{\pi}{2}$ rad. This development in look angle eases flight restrictions and makes the use of airborne radar more attractive. It was assumed that the airborne radar would be a range optimized phased array X band system. The range would be accurate to ± 3 m, and the angular accuracy is $\pm 3.927 \times 10^{-3}$ rad. The phased array radar is ideal for a landing system because failure of some of the antenna elements slightly degrades the antenna performance, and the

7

failure is not catastrophic. In addition, a phased array radar can take over such other duties as weather surveillance, midcourse navigation, and collision avoidance during other portions of the flight.

Because of ground return, the airborne radar would function much better if some form of runway enhancement were used. A semiactive reflector that introduces a small frequency shift in the return signal would permit the correct signal to be distinguished from the ground return. Such a reflector was assumed in the study and it was located 900 m down the runway from the touchdown point and 100 m off the center line.

The inertial measuring for the autoland system measures linear accelerations which are integrated to obtain the velocity vector of the airplane. The IMU also measures the orientation of the airplane in space and is equipped with rate gyros and angular accelerometers that measure the angular rates and accelerations about the body reference axes. Inasmuch as the radar, through the measurement of the range rate vector, can also be used to determine the airplane velocity vector, these units can be used to check each other.

Coordinate Systems and Transformations

Five coordinate systems were used in the autoland system; these are

(1)   inertial coordinates η_j

(2)   quasi inertial coordinates z_j

(3)   airplane coordinates y_j

(4)   radar coordinates x_j

(5)   runway coordinates ζ_j

The subscript j in the symbol for the coordinate takes on the values 1, 2, or 3, the values denoting a specific axis. When $j = 1$, the axis corresponds to the x-axis of a usual x,y,z coordinate system. Similarly, $j = 2$ corresponds to the y-axis and $j = 3$, the z-axis. The transformations between these coordinate systems are given in appendix C.

The inertial coordinates do not rotate and are forced to translate with the airplane. The η_1-axis has the same direction as the runway center line. The inertial coordinates and their relationship to the quasi inertial coordinates and airplane coordinates are shown in figure 2(a). The quasi inertial coordinates are rotated by the angle ψ, obtained by a positive rotation about the η_3-axis. The z_1-axis now points in the direction of flight. The airplane coordinates are related to the quasi inertial system through the two additional angles θ, obtained by a positive rotation about the z_2-axis, and ϕ, obtained by a positive

8

rotation about the y_1-axis. The rotations through the angles ψ, θ, and ϕ are the standard Euler angles and are calculated by the formulas in appendix B.

The radar coordinate system is related to the airplane coordinates by the two angles θ_a and θ_e. The angle θ_a is obtained by a positive rotation about the y_3-axis and θ_e, by a positive rotation about the y_2'-axis. The rotations are taken in the order given. The angles θ_a and θ_e are calculated by the formulas given in appendix B. The range is measured in radar coordinates and is a single component vector directed along the x_1-axis and is positive from the airplane to the target. This places the origin for the radar coordinates at the center of the radar antenna. The radar coordinates translate with the airplane.

The runway coordinates use the touchdown point as a fixed origin and the ζ_1 is positive toward the far end of the runway. These coordinates, except for $j = 3$, are the negative of the inertial system. This system is used only for the reporting of the results.

The Turn Computer

The purpose of the turn computer is to provide a bank angle command that is used to control the roll of the airplane and the rotation about the y_2 body axis to produce a coordinated banked turn that will reduce the heading and runway centering errors to zero. These two errors must be brought to zero simultaneously. A typical situation to be handled by the turn computer is shown in figure 3. The airplane is located off to one side of the runway with an incorrect heading. The heading error is $\psi_c - \psi$, where ψ_c is the runway heading and in this study was assumed to be zero. The runway centering error is given by $\theta_{AC} - \theta_{AA}$. The turn command must reflect the total error to be eliminated which is the sum of these individual errors. The total error E may be written as

$$E = \left(\psi_c - \psi \right) + k_1 \left(\theta_{AC} - \theta_{AA} \right) \tag{1}$$

where k_1 is a gain introduced so that the weight given to each part of the total error could be varied. The total error was made proportional to a bank angle command ϕ_c

$$\phi_c = k_2 \left[\left(\psi_c - \psi \right) + k_1 \left(\theta_{AC} - \theta_{AA} \right) \right] \tag{2}$$

where k_2 is a gain that determines the proportionality between the command bank angle and the total error.

For the condition shown in figure 3, ψ and θ_{AC} are positive, θ_{AA} is negative, $\psi_c = \psi_r = 0$, and the airplane must roll negatively in order to direct the normal acceleration to turn it in the correct direction to eliminate the error. The heading error for this case is negative and the runway centering error is positive; thus, there is a value of k_1,

9

called $\bar{k}_1$, that makes the total error zero. There are two cases to consider: $k_1 < \bar{k}_1$ and $k_1 \geqq \bar{k}_1$.

The case $k_1 < \bar{k}_1$.- When $k_1 < \bar{k}_1$, an error exists when the turn computer is turned on at the start of the landing maneuvers and $\left| \psi_c - \psi \right| > k_1 \left| \theta_{AC} - \theta_{AA} \right|$. As $\psi_c - \psi$ is negative and $k_1 \left(\theta_{AC} - \theta_{AA} \right)$ is positive, the sign of the total error is correct and equation (2) produces a roll command that turns the airplane to reduce the total error to zero. Once the initial error has been brought to zero and ϕ_c returns to zero, the forward motion of the airplane causes $k_1 \left(\theta_{AC} - \theta_{AA} \right)$ to increase. Because $k_1 \left(\theta_{AC} - \theta_{AA} \right)$ now dominates the total error, the airplane turns away from the runway. This motion causes $\psi_c - \psi$ to increase and continues until $\psi_c - \psi$ becomes large enough to again dominate the command and turn the airplane back toward the runway. This interaction produces a snaking motion that is totally unacceptable and the airplane does not line up for a landing because both errors are not satisfied simultaneously.

The case $k_1 \geqq \bar{k}_1$.- For $k_1 = \bar{k}_1$, the total error is zero and no immediate turn takes place. However, the forward motion causes no change in $\psi_c - \psi$ but increases $\theta_{AC} - \theta_{AA}$ and thus develops a total error. However, the total error is positive and would command a positive roll instead of a negative one. If k_2 is negative, a roll in the proper direction takes place and the subsequent motion satisfies both the heading error and the runway centering error and the airplane motion becomes a smooth curve toward the target point. When $k_1 > \bar{k}_1$, a similar process takes place.

The total error that is controlling the airplane has an interesting physical interpretation. If $k_1 = \bar{k}_1$, the total error is zero, no turning takes place, and the curvature is zero. However, if k_1 is very large with respect to $\bar{k}_1$, the total error is large, the turn becomes very sharp, and the curvature becomes large. Thus, the total error, which represents the amount the tangent of a space curve must be turned to zero the error, is related to the instantaneous curvature of a space curve. This relationship between the total error and the curvature of a space curve illustrates the critical nature of the gain k_1, as it is this gain that determines the curvature and the sharpness of the turn.

Experience with the use of equation (2) showed that better turns could be obtained if $\dot{\psi}$ was used as a feedback into the turn command. With this feedback, equation (2) becomes

$$ \phi_c = k_2 \left[\left(\psi_c - \psi - k_3 \dot{\psi} \right) + k_1 \left(\theta_{AC} - \theta_{AA} \right) \right] \tag{3} $$

Equation (3) with k_2 negative was adopted as the basic guidance law for the algorithm of the turn computer. This guidance law can be used by itself or combined with other guidance laws for calculating turn commands. In an algorithm with combined commands,

10

equation (3) is always used for the final phase of the landing. Both the basic turn algorithm and a combined turn algorithm were used in this study. The combined turn algorithm used pure heading turns and straight line segments in combination with the basic turn algorithm. The details of the basic and combined turn algorithms are given in appendix D.

The Letdown Computer

The purpose of the letdown computer is to determine the required flight-path angle for the airplane, generate turn coordination information, and provide a pitch rate signal for the elevator autopilot. This computer also provides the signal for lowering the flaps. The geometry used to determine the flight-path command γ_c is shown in figure 4. If H > 20,

$$\gamma_c = -\tan^{-1} \frac{H - 20}{\left\| \vec{R}_H + \vec{R}_{RTD} \right\|} \tag{4}$$

and if H < 20,

$$\gamma_c = -\tan^{-1} \frac{H}{275.0} \tag{5}$$

Equation (5) was used to compute γ_c for flaring the airplane. Because these flight-path command angles are continuously calculated and referenced to the present position of the airplane, disturbances to the airplane positions are compensated for in the γ commands. The command γ_c was used in the following equation to compute a pitch-rate command for the elevator autopilot:

$$q_c = -k_5 \left[k_{14} \left(\gamma_c - \gamma_o \right) + \frac{g \tan \phi_c \sin \phi_o}{V_T} + \dot{\alpha} \right] - \int_0^t \left(\gamma_c - \gamma_o \right) dt \tag{6}$$

where γ_o is given by equation (F5). This first term in equation (6) is the γ error term that supplies the principal control input for the letdown. The last term, the integral of the γ error, is necessary so that the system will have zero steady-state error. The term

$$\omega = \frac{g \tan \phi_c}{V_T} \tag{7}$$

supplies turn coordination information, and the $\sin \phi_o$ term converts this information to the airplane body axis y_2. The commanded bank angle is used instead of the actual bank angle to give some anticipation to the turn coordination because the q response of the airplane is slow.

The $\dot{\alpha}$ term comes from the equation for the turning rate of an airplane velocity vector in space, which is

$$\dot{\vec{T}} = \frac{1}{V^2} \vec{V} \times \frac{d\vec{V}}{dt} \tag{8}$$

and has a component $q - \dot{\alpha}$ about the y_2 body axis. This component and ω both specify the rotational rate about the y_2 body axis for a coordinated turn. These terms may be equated and solved for a pitch rate, which accounts for the $\dot{\alpha}$ term in equation (6). Equation (6) is the principal part of the letdown algorithm used in this study, the details of which are given in appendix E. The γ_c signal from this algorithm was used to control the flaps. When γ_c became less than zero or attained a specific value, the flaps were lowered.

Speed Control

Speed control was achieved through the use of a digital thrust control system. The following equation was used to compute change in thrust required to eliminate a speed error:

$$\Delta T = k_6 \left(V_c - V_T \right) - m\dot{u} \tag{9}$$

where

$$k_6 = V_c \left(28.131 + 58.973 \delta_f \right) \tag{10}$$

If the ΔT calculated by equation (9) is added to the present thrust T, the new total thrust is $T + \Delta T$. The positions in time of T and $T + \Delta T$ were found in table I. The difference in the times associated with these two thrusts indicated how long it should take to change the thrust from T to $T + \Delta T$. The change in thrust ΔT was added linearly over this time. After the thrust was changed, the thrust controls were shut down for 4 sec. At the end of 4 sec, V_T and $\dot{u}$ were sampled to determine whether they were within the control system deadband. The deadband for V_T was ± 1.0 m/sec and for $\dot{u}$ was ± 0.1 m/sec^2. If the errors were within the deadband, no more changes were made. However, if one or both errors were outside the deadband, thrust changes were made until the error entered the deadbands.

Autopilots and Servos

The autopilots shown in the block diagram of figure 1 are, with the exceptions of the roll autopilot, self-explanatory. In the roll autopilot, ϕ_E was limited in order to hold down the roll rate of the airplane. The servos are also shown in figure 1 and all necessary data are given there. The necessary integrations on the digital computer were performed using the state variable convolution method. As the typical power servo of a large transport aircraft has a natural frequency of about 30 Hz and a damping ratio greater than 1.0, a

12

second-order servo with these characteristics can be adequately represented by a first-order system. All servos were rate and displacement limited. A rate limit of ±0.34907 rad/sec was used for all servos. The displacement limit varied with the surface, the δ_{a_i} limit was ±0.34907 rad, the δ_e limits were 0.26180 rad and -0.43633 rad, the stabilizer limit was ±0.34907 rad, and rudder deflection was limited to ±0.5236 rad. The rate and displacement limits were rarely, if ever, encountered.

The output of the aileron servo δ_{a_0} did double duty. In addition to actuating the ailerons, this variable was also used to actuate the spoilers for roll control (see appendixes D and F). If δ_{a_0} exceeded 0.1745 rad, the spoilers were actuated. Because of the rapidity of spoiler actuation, no servos were used.

The Airplane

The last block of figure 1 represents the airplane. The airplane considered in this study was a large, four-engine subsonic jet transport with a mass of 90 719.4 kg. In the study, the airplane was represented by the six-degree-of-freedom equations of motion referred to principal body axes. Linear aerodynamics were used. The physical and aerodynamic characteristics of the airplane are given in appendix F.

Comments on the Autoland System

The operation of the autoland system was studied for the initial conditions described by the box labeled "autoland system" in figure 5. It was assumed that the airplane was on a course that would cause it to intercept the boundaries of this volume and, as the airplane entered this volume, the automatic landing system would be turned on and a landing effected. It is not necessary to actuate the landing system when the outermost boundary is crossed; it may be turned on any time after this boundary is crossed but must be actuated before the boundary closest to the runway is crossed. The operation of the system is not restricted to the volume shown. The only restriction is that the airplane be so positioned that good radar data can be obtained. In the case of an airborne radar, this would be about 40 km from the touchdown point, and also the reflector must be in the field of view of the radar. Several runs were made from greater distances than those shown for the autoland system. The same maneuvers as for the normal distances were noted, together with long periods of straight flight.

It is interesting to compare the volume of operation of the autoland system with that of the current instrument landing system (ILS) system. This comparison is shown in figure 5; while the autoland system uses a rectangular prism for its zone of operations, the ILS uses a pencil type volume with very low glide slope. Automatic landing systems have been developed for use with the ILS type landing system, and one is described in reference 2. These are beam rider type systems and cannot make the steep curved approaches of which the autoland system described in this report is capable.

RESULTS AND DISCUSSION

The automatic landing system discussed in the previous section was programed to be studied on a digital computer. In the program, all integrations except for the servos were done with the Adams-Bashforth prediction method. The state variable convolution method was used when performing integration connected with the servos.

The results of the study of the automatic landing system are summarized in table II. The first 26 entries give the touchdown conditions for various initial conditions for an initial altitude of 540 m. The remaining entries are cases included to demonstrate changes in initial altitude, the use of straight line segments with the turn computer, and other special cases. Figures 6 to 11 illustrate a few of the first 26 cases. Generally speaking, the airplane executed two basic types of flight path to the landing, a sweeping curve as shown in figure 6 or a compound curve as shown in figure 7. Inasmuch as all trajectories were variations of these basic ones, airplane responses are given for these two; all other examples are confined to ground tracks as the altitude tracks for the first 26 cases do not show much variation except in the glide-slope angle.

The two basic ground tracks with the altitude tracks and airplane responses are shown in figures 6 and 7, which correspond to cases 9 and 17, respectively, of table II. The ground tracks are smooth curves that go from the initial position of the airplane to the touchdown point which is located at 0,0. Two altitude tracks are shown on figures 6(b) and 7(b), the one with the crossmarks being the desired altitude track and the other, the actual altitude track of the airplane. The desired altitude track is for reference only and does not represent a feed forward command for the airplane. The airplane responses for the parameters ϕ, β, α, θ, γ, and the heading angle ψ, presented in figures 6 and 7 are smooth and relatively well damped and are considered satisfactory. The lateral acceleration encountered during a typical landing maneuver was well controlled and in most cases was equal to or less than 0.01g; however, when the bank angle reached its limit, the maximum lateral acceleration was 0.046g. In both cases, the values quoted are the peaks of long period oscillations that occur during maneuvers. The control surface motions, which are not shown, did not reach their rate or displacement limit; and the spoilers, which were coupled to the aileron displacement, rarely actuated.

Figures 8 to 11 illustrate some interesting conditions that this system can handle. Figure 8 shows the ground track for the initial condition ζ_1 = -6000 m, ζ_2 = -2000 m, H = 540 m, and $\psi = \frac{\pi}{2}$ (case 1 of table II). For this case, the airplane crossed the center line of the runway before it had completed its turn but was able to reverse itself and make a satisfactory landing, showing that the system can handle an overshoot. Figure 9 is a ground track for the same position, except that the airplane has a heading of $-\frac{\pi}{6}$ and is moving away from the runway center line (case 4 of table II). For this case, the airplane was able to make a satisfactory landing. Based on airborne radar view angles

14

assumed for this system, the system can handle heading angles that permit a course away from the runway between -0.2368 rad and 0.7785 rad; the exact value is, of course, dependent on the initial ζ_1, ζ_2 position of the airplane. Figures 10 and 11 illustrate the ability of the system to handle the initial conditions $\zeta_1 = -3000$ m, $\zeta_2 = \pm 4000$ m, and H = 540 m and are cases 24 and 22, respectively, of table II.

The first 26 cases of table II illustrate the capabilities when the landing system was turned on as the airplane crossed the boundaries of the box marked "autoland" in figure 5. In the first 20 cases, satisfactory touchdown conditions were obtained. In cases 21 to 26, satisfactory touchdown conditions were not always obtained; the satisfactory cases of this group, for example, cases 22 and 25, represent limiting cases for the method used for determining the gains k_1 and k_2.

The gain k_1 is position dependent and is redetermined each time the airplane starts a new turn. For case 9, figure 6, only one turn is required to aline the airplane for landing and k_1 was calculated only once at $t = 0$. In case 17, figure 7, two values of k_1 were required. The first value was calculated at the beginning of the landing maneuver, $t = 0$, and the second at about 38 sec. This point is labeled "k_1 switch" in figures 7(a) and 7(d). Equation (D6) was always used to determine the first value of k_1. The subsequent values of k_1 may be calculated using either equation (D6) or equation (D11). The gain k_1 was changed when either the roll angle ϕ_o or heading angle rate became zero. Suitable logic based on $\psi_c - \psi$ and $\theta_{AC} - \theta_{AA}$ prevented gain changes after the airplane was alined with the runway and at the start of each turn after k_1 had been set.

As used in the basic roll algorithm, the gain k_2 is also initial condition dependent and, for the most part, satisfactory results were obtained when k_2 was determined by using equation (D7). For some of the more extreme initial conditions, cases 21 to 26, satisfactory landings were not always achieved. Setting the ratio $\dfrac{k_4}{k_1} = 2.02$ in equation (D7) and applying it to initial conditions for case 23 produced very satisfactory landing conditions. The roll error at touchdown was little changed, but the heading error improved by a factor of 10^{-3} and the ζ_2 error was improved by a factor of 3. These results indicate that the selection of the constant k_4 in equation (D7) is important for achieving a satisfactory landing. The very limited results available on this problem indicate that a change in the value of k_4 from about 3.8 to 4.0 when k_1 is determined for the second time is necessary. Based on the roll-angle time history, the rerun of case 23 with $\dfrac{k_4}{k_1} = 2.023$ indicates that this case and cases with similar initial conditions represent limiting conditions for this autoland system and the airplane considered.

Optimization methods were not employed to determine k_1 and k_4. It is thought that little would be gained by applying such methods to the determination of k_1; however, optimization methods may offer a fruitful approach to the determination of k_4.

The results for the vertical plane show that in general the airplane was slightly pitched up at touchdown and the touchdown point was in error between 39.3 m (short) and 367 m (long) with respect to the desired touchdown point. Part of this overshoot was caused by an initial altitude that was too high for the longitudinal control system that was limited to a 0.10422 rad glide slope. When the altitude was reduced, the overshoot was dramatically reduced, as can be seen by comparing cases 21 and 27. Two other factors also affect the overshoot in this system; the first is the distance along the ground track which affects the time to touchdown and the second is the flare computer algorithm. In this system, the ground track is determined by turn calculation and varies with the initial conditions at the start of the turning and the values calculated for k_1 and k_4. In some cases, the path was such that there was sufficient time and distance to achieve a touchdown close to the landing point and in others, not. The overshoots produced by this factor are not large, about 50 m, compared with runway length and can be tolerated.

Equation (5) was used as the algorithm for the flare computer. This algorithm affects both the overshoot of the desired touchdown point and the vertical speed at touchdown. The vertical speed at touchdown for the landings listed in table II varied from 0.34 m/sec to 3.2 m/sec. Vertical touchdown speed should not exceed 0.5 to 0.6 m/sec.

One of the worst cases for overshoot and vertical touchdown speed is case 23. In this case the overshoot was 367 m and the vertical touchdown speed was 3.2 m/sec. The flare used in this run was controlled by the output of equation (5). In order to improve these conditions, a new equation to compute γ_c during the flare was developed. This equation, which is based on predicting the impact by using the flight-path angle at a 20 m altitude is

$$\gamma_c = \tan^{-1}\left(\frac{H \tan \gamma_{20}}{20}\right) \tag{11}$$

where γ_{20} is the flight path angle at an altitude of 20 m. Case 23 was rerun using equation (11) to control the flare. This run, listed as case 34 of table II, shows great improvement in the vertical touchdown speed which is now 0.58 m/sec. However, the overshoot was increased by about 80 m, giving a total overshoot of about 450 m. As touchdown occurred in the first third of the 3000 m runway, this overshoot from the desired touchdown point was not considered critical.

Cases 28 and 30 were included to show how the system operates at low altitude. The initial conditions used were $\gamma_1 = -3000$ m, $\gamma_2 = \pm4000$ m, H = 200 m, and $\psi_i = \pm\frac{\pi}{2}$. For the low altitude condition, the turn control functioned in the usual manner. The

16

longitudinal control maintained constant altitude until γ_c reached a predetermined value of -0.073 rad. When this value was reached, the longitudinal control system initiated a normal letdown. This low altitude letdown is compared with a normal letdown in figure 12, in which altitude versus time traces for cases 21 and 28 are shown.

As was pointed out in the previous section, the basic turn command can be combined with other commands to guide the airplane to a landing. Cases 31 and 32 combine the basic roll command with straight-line segments and free turns. The ground track for case 31 best illustrates this combination. This ground track, presented in figure 13, starts with a turn to a specified heading and is followed by a period of level flight until η_2 reaches the value given by equation (D10). At this point, ψ_c was set equal to the runway heading and k_1 was calculated by equation (D11). Equation (D6) cannot be used with this turn algorithm to compute k_1. The airplane made a smooth turn onto the runway and landed. This combined form of lateral control produced no significant changes in the letdown to the runway or in the airplane responses. When compared with case 9, the only significant change introduced other than the form of the ground track is a reduction of 11.4 sec in the time to land.

The forward speed of the airplane was controlled during the landing maneuver. This involved changing from the approach speed of 77.12 m/sec to 72.43 m/sec, the landing speed. This was accomplished through the speed control system described in the previous section. Typical speed and thrust time histories for the landing maneuvers are shown in figure 14(a) for case 27. This case has a time to land of about 80 sec. When longer flight times were involved, the only major change was an increase of flight time at the lower speed. For the typical case the speed change command and the command to lower the flaps from 0.436 rad to 0.872 rad were given at the start of the landing maneuver. A small decrease in speed was followed by an increase to about 78.5 m/sec, this surge being caused by the airplane pitching over onto the letdown trajectory. The speed surge was eliminated in approximately 10 sec and speed was gradually reduced to 73.4 m/sec, the top of the deadband, by 64 sec. At 77 sec, the engines were idled for the touchdown. The $\dot{u}$ term in equation (9) is important; without this term, which supplies damping, the speed excursions, although smooth, were large, the speed dropping to about 60 m/sec halfway through the maneuver followed by an overshoot. The speed and thrust curves for case 28 of table II are shown in figure 14(b). As in case 27 the command to change the speed and flap setting was given at the start of the landing maneuver, $t = 0$. Because γ_c had to be -0.073 rad or less, the letdown did not start until 41 sec had elapsed (see fig. 12(b)). During the first 41 sec the speed was reduced to 71.9 m/sec; but as the letdown started, a large speed surge occurred that would be intolerable in the landing maneuver. This speed variation occurred because of lack of coordination between speed change commands, flap lowering commands, and start of letdown. The command sequences were modified so that these commands occurred at the same time, and the resulting speed and thrust curves

are shown in figure 14(c), case 33 of table II. As can be seen, the unacceptable speed variations were eliminated, which illustrated the importance of coordination of speed reduction, flaps, and letdown.

The results presented in this section are all for a bland environment, that is, no noise and no winds. Some preliminary results for head winds and cross winds with shear have been obtained for a maximum wind speed of 25.80 m/sec. These results show that there is no appreciable effect on the system, although a decrab control system would considerably relieve the touchdown stresses. As pointed out in the introduction, the purpose of this study was not to develop an automatic landing system that could be put into an airplane, but to investigate the concept of an airborne autoland system that, when combined with a scanning microwave landing system, would provide a self-contained system with an independent landing monitor. The system studied provides satisfactory airplane responses and landings over a wide range of initial conditions (see table II) and is considered a feasible system. Although the system functioned well, the results indicate that more work is necessary to refine the methods for determining the gains k_1 and k_2 in the turn algorithm and the flare algorithm, equation (5) or equation (11), of the letdown subsystem. Optimization methods might be of value in such a study.

CONCLUDING REMARKS

An automatic landing system for aircraft that takeoff and land in a conventional manner has been studied. This system obtains its data from an airborne inertial measuring unit and a radar that may be either airborne or located on the ground. When the two radars are combined, as could be done with the microwave landing system (MLS), a system with an independent landing monitor results. This system is capable of executing steep, curved approaches while changing speed from approach to landing conditions. Landing maneuvers that give satisfactory landings may be started as close as 3000 m from the touchdown point and over a wide range of heading angles with respect to the runway. The results show that the automatic landing system studied is a feasible system. System gains were not optimized for this study; however, the use of optimization methods for gain calculation and an improved flare algorithm should improve the system response.

Langley Research Center,
    National Aeronautics and Space Administration,
        Hampton, Va., April 19, 1974.

APPENDIX A

SIGNALS FROM A GROUND LOCATED TRACKING RADAR

As pointed out in the body of the report, the autoland system can use data from either an airborne radar or a tracking radar located on the ground. The model for the system discussed in appendix B is based on the use of an airborne radar. Appendix A discusses an interface that will permit the use of data from a ground radar.

It is assumed that the ground radar is referenced to the runway center line so that radar azimuth angles can be read 0 to $\pm\pi$ or 0 to 2π rad and converted to the former. To insure good data, the airplane should be equipped with a nose reflector so that the return will come to a discrete point. The data required from the ground radar are the range, range rate, the elevation angle, and the azimuth angle. This data would be transmitted to the airplane where it would pass through an inertial smoothing process (see ref. 9). After smoothing, the data would have to be preprocessed before going to the airplane navigation system. The preprocessing is quite simple; the range R can be used without modification as can the range rate. The azimuth angle for the ground radar θ_{AG} is measured in a plane that is parallel to the z_1, z_2 plane, and the elevation angle for the ground radar θ_{EG} is measured in a plane perpendicular to this plane. The required angles θ_{AA} and θ_{EE} are obtained as follows from θ_{AG} and θ_{EG}:

$$\theta_{EE} = -\theta_{EG} \tag{A1}$$

and

$$\theta_{AA} = \theta_{AG} - \psi + \psi_r \tag{A2}$$

The transformations and equations of the guidance system can now be used to obtain the information required to guide the airplane to a landing.

AIRBORNE RADAR AND INERTIAL MEASURING UNIT

The radar was modeled by the following equations:

$$R = R_i + \int_0^t \dot{R}_{x_1} \, dt \tag{B1}$$

$$\theta_a = \theta_{a_i} + \int_0^t \left[-\frac{\dot{R}_{x_2}}{R} \sec \theta_e - r - \left(q \sin \theta_a + p \cos \theta_a \right) \tan \theta_e \right] dt \tag{B2}$$

$$\theta_e = \theta_{e_i} + \int_0^t \left(\frac{\dot{R}_{x_3}}{R} - q \cos \theta_a + p \sin \theta_a \right) dt \tag{B3}$$

The range vector is a vector that connects the vehicle with the target, and its direction with respect to airplane coordinates is given by θ_a and θ_e. The range rates $\dot{R}_{x_1}$, $\dot{R}_{x_2}$, and $\dot{R}_{x_3}$ are obtained by transforming the airplane velocity component along and perpendicular to the range vector. The integrand of equations (B2) and (B3) are $\dot{\theta}_a$ and $\dot{\theta}_e$, respectively.

The angles θ_a and θ_e are the radar angles between the airplane axes and the line of sight. The angle θ_a is the azimuth angle and θ_e is the elevation angle. The order of rotation is first θ_a and then θ_e. The positive direction is the same as for the Euler angles which follow.

The standard Euler angles which are used in the transformations presented in appendix C were also used to represent the angular output of an inertial measuring unit. Because the angular displacements were not expected to exceed 0.52360 rad, no singularities would be experienced in computing the Euler angles. Therefore, the Euler angles could be computed by integrating their rates. The equations used to compute the Euler angles are

$$\psi = \psi_i + \int_0^t \left[\left(q \sin \phi + r \cos \phi \right) \sec \theta \right] dt \tag{B4}$$

$$\theta = \theta_i + \int_0^t \left(q \cos \phi - r \sin \phi \right) dt \tag{B5}$$

$$\phi = \phi_i + \int_0^t \left[p + \left(q \sin \phi + r \cos \phi \right) \tan \theta \right] dt \tag{B6}$$

The integrands of the above equations are $\dot{\psi}$, $\dot{\theta}$, and $\dot{\phi}$; and ψ_i, θ_i, and ϕ_i are the initial values of these angles.

The angle ψ represents the heading angle of the airplane, and θ and ϕ are the pitch and roll angles, respectively. Equations (B4) and (B6) are based on the standard aeronautical rotation order of ψ, θ, and ϕ.

APPENDIX C

COORDINATE TRANSFORMATIONS

The basic coordinate system used is an inertial system that has the η_1-axis pointed in the same direction as the runway and the η_3-axis positive downward. The η_2-axis is perpendicular to the η_1,η_3 plane positive in the direction for a right-handed coordinate system. This system was fixed in the airplane at the center of mass and translated with the airplane. The runway coordinates ζ_j were centered at the landing point and are related to η_j by

$$\zeta_1 = -\left(\eta_1 - 900\right)$$

$$\zeta_2 = -\left(\eta_2 - 100\right)$$

$$\zeta_3 = \eta_3$$

and the altitude is $H = -\zeta_3$. The third set of coordinates was the z_j system. This system was rotated from the inertial system by the angle ψ. The transformation between the two coordinate systems is

	z_1	z_2	z_3
η_1	$\cos\psi$	$-\sin\psi$	0
η_2	$\sin\psi$	$\cos\psi$	0
η_3	0	0	1

(C1)

The airplane body axis system of coordinates y_j was related to the z_j system by the following transformation:

	y_1	y_2	y_3
z_1	$\cos\theta$	$\sin\theta\sin\phi$	$\sin\theta\cos\phi$
z_2	0	$\cos\phi$	$-\sin\phi$
z_3	$-\sin\theta$	$\cos\theta\sin\phi$	$\cos\theta\cos\phi$

(C2)

These two transformations, when combined, give the usual transformation between inertial and airplane coordinates. The angles ψ, θ, and ϕ of the transformations (C1)

and (C2) are the usual Euler angles. The next transformation used is between airplane axes and the radar axes. This transformation is

	x_1	x_2	x_3
y_1	$\cos \theta_a \cos \theta_e$	$-\sin \theta_a$	$\cos \theta_a \sin \theta_e$
y_2	$\sin \theta_a \sin \theta_e$	$\cos \theta_a$	$\sin \theta_a \sin \theta_e$
y_3	$-\sin \theta_e$	0	$\cos \theta_e$

where θ_a and θ_e are angles that define the center line of the radar beam and are measured in the same sense as ψ and θ. The angle θ_a is measured in the y_1, y_2 plane and θ_e is measured from the y_1, y_2 plane to the beam center line. The angles θ_a and θ_e are generated in the radar model.

APPENDIX D

TURN ALGORITHM

Basic Turn Algorithm

The basic equation of the turn algorithm is

$$\phi_c = k_2\left[\left(\psi_c - \psi - k_3\dot\psi\right) + k_1\left(\theta_{AC} - \theta_{AA}\right)\right]$$ (D1)

where ψ_c is the desired or command heading angle, ψ is the heading angle of the airplane obtained from equation (B4), and θ_{AC} and θ_{AA} were computed from the following equations:

$$\theta_{AC} = \tan^{-1}\left(\frac{100}{R_{z_1}}\right)$$ (D2)

$$\theta_{AA} = \tan^{-1}\left(\frac{R_{z_2}}{R_{z_1}}\right)$$ (D3)

The output of equation (D1) was limited in order to prevent too large bank angles. The limiting was as follows:

$$-\phi_\ell \leqq \phi_c \leqq \phi_\ell$$

If $\eta_2 \geqq 0$, $\phi_\ell = \frac{\pi}{9}$; if $\eta_2 < 0$, $\phi_\ell = \frac{5\pi}{36}$.

The important part of the use of equation (D1) is the calculation of the gains k_1 and k_2. Both of these gains are dependent on initial conditions; in fact, k_1 must be recalculated at the start of turns. To illustrate that point, one value of k_1 would be required for the case shown in figure 6. For the case shown in figure 7, it is necessary to recalculate k_1 at about 40 sec where the airplane starts a turn in the opposite direction. The cue for recalculating k_1 was either ϕ or $\dot\psi$ changing sign. The gain k_2 was much simpler to set and the method used will be given first. The gain k_2 was calculated from the equation

$$k_2 = \frac{k_4}{k_1}\exp\left(-\left|\psi_c - \psi\right|\right)$$ (D4)

with

$$k_4 = 4.8 \quad \text{if} \quad \left| \psi_i \right| < \frac{\pi}{2} \quad \text{and} \quad 3.0 \text{ if} \quad \left| \psi_i \right| = \frac{\pi}{2}$$

The following method was used to calculate the gain k_1:

$$\left. \begin{aligned} \overline{R}_{z_1} &= \eta_1 \cos \left(K_1 - \psi \right) + \eta_2 \sin \left(K_1 - \psi \right) \\ \overline{R}_{z_2} &= \eta_1 \sin \left(K_1 - \psi \right) + \eta_2 \cos \left(K_1 - \psi \right) \end{aligned} \right\} \tag{D5}$$

where $K_1 = \frac{\pi}{2}$ for $\eta_2 > 0$ and $K_1 = -\frac{\pi}{2}$ for $\eta_2 < 0$. The $\overline{R}_{z_1}$ and $\overline{R}_{z_2}$ were used in equations (D2) and (D3) to compute $\bar{\theta}_{AC}$ and $\bar{\theta}_{AA}$ which were used to determine k_1 from the following equation:

$$k_1 = \left| \frac{\psi_c - K_1 - k_3 \dot{\psi}}{\bar{\theta}_{AC} - \bar{\theta}_{AA}} \right| \tag{D6}$$

This equation was used to calculate k_1 at the beginning of the landing maneuver $\left(k_1 \right)_1$ and when either ϕ_0 or $\dot{\psi}$ changed sign $\left(k_1 \right)_2$. This determination of k_1 was subject to the following restrictions that are based on experience on the computer:

(1) If $\psi_i = \pm \frac{\pi}{2}$, only $\left(k_1 \right)_1$ is calculated

(2) If $\eta_2 > 0$, $\left(k_1 \right)_1$ or $\left(k_1 \right)_2 \cong 1.483$

(3) If $\eta_2 < 0$, $\left(k_1 \right)_1$ or $\left(k_1 \right)_2 \cong 1.524$

(4) If $\left(k_1 \right)_2 > \left(k_1 \right)_1$, use $\left(k_1 \right)_1$ in place of $\left(k_1 \right)_2$.

After $\left(k_1 \right)_2$ had been determined for the first time, logic was used to block further computation of this gain.

The gain k_2, which is also initial condition dependent, was calculated by

$$k_2 = \frac{k_4}{k_1} \exp \left(-\left| \psi_c - \psi \right| \right) \tag{D7}$$

where $k_4 = 3.0$ if $\left| \psi_i \right| = \frac{\pi}{2}$ or $k_4 = 4.8$ if $\left| \psi_i \right| < \frac{\pi}{2}$.

Combined Turn Algorithm

In the combined turn algorithm used in this study, straight line segments were combined with equation (D1). At the start of a landing maneuver, equation (D1) was used with $k_1 = 0$ and k_2 positive and given by

$$k_2 = 4.0 \left[\exp\left(t - 8.0\right) \right] \tag{D8}$$

to turn the airplane to a desired heading angle given by

$$\psi_c = \tan^{-1}\left(\frac{\eta_{2_i}}{\eta_{1_i} - N} \right) \tag{D9}$$

The exponential in equation (D8) is used to prevent too rapid a buildup of the roll angle and the 8.0 is the number of seconds required for the gain to reach its full value. The 8.0 is not a fixed number but can be adjusted as required. Logic was incorporated to limit k_2 to 4.0. The N in equation (D9) is the intercept on the runway center line of the new course and can, within limits, be set as desired. In this study, N was set at 3000 m. The value assigned to N should be less than η_{1_i} but should not be much less than 3000 m; precise limits have not been established.

After the airplane had turned through the angle ψ_c, given by equation (D9), the roll angle command was set to zero and kept at that value until

$$\eta_2 = \frac{\left(V_{max} + V_{min}\right)^2}{g \tan \phi_\ell} \tag{D10}$$

At this point ψ_c was set equal to the runway heading and k_1 was calculated by

$$k_1 = \frac{\left| \psi_c - \psi - k_3 \dot{\psi} \right|}{\left| \theta_{AC} - \theta_{AA} \right|} \tag{D11}$$

where ψ and $\dot{\psi}$ are the actual ψ and $\dot{\psi}$ of the airplane calculated by equation (B4) and θ_{AC} and θ_{AA} are calculated from the output of radar algorithm by equations (D2) and (D3). In the combined turn algorithm, k_1 had to be greater than or equal to 1.2 and k_2 was set equal to 4.0. Equation (D1) was used to determine ϕ_c.

Two equations have been presented for the calculation of the gain k_1. These are equations (D6) and (D11). Equation (D11) is the general version and it must be used to determine k_1 for the combined turn algorithm and may be used in the basic turn algorithm to calculate $\left(k_1\right)_2$. Equation (D6) is a special form of equation (D11) and was necessary in the basic turn algorithm for the calculation of $\left(k_1\right)_1$.

The output of equation (D1), ϕ_c, was used to compute

$$\phi_E = k\left(\phi_c - \phi_o\right) \tag{D12}$$

and the condition

$$-0.45 \leq \phi_E \leq 0.45 \tag{D13}$$

26

was imposed. This ϕ_E was used as indicated in the block diagram (fig. 1) to obtain a δ_{a_O} for the airplane.

Calculation of Spoiler Deflection Angles

The spoiler deflection was tied to the aileron deflection through the following equations:

$$\text{If} \quad \delta_{sp} < -\frac{\pi}{3}, \quad \delta_{sp} = -\frac{\pi}{3}$$

$$\text{If} \quad \delta_{a_O} < -0.15708, \quad \delta_{sp} = -1.08385 - 6.9\delta_{a_O}$$

$$\text{If} \quad -0.15708 \leqq \delta_{a_O} \leqq 0.15708, \quad \delta_{sp} = 0$$

$$\text{If} \quad \delta_{a_O} > 0.15708, \quad \delta_{sp} = 1.08385 - 6.9\delta_{a_O}$$

$$\text{If} \quad \delta_{sp} > \frac{\pi}{3}, \quad \delta_{sp} = \frac{\pi}{3}$$

APPENDIX E

LETDOWN ALGORITHM

The basic command for the pitch autopilot is a pitch rate given by

$$q_c = -k_5 \left[k_{14}(\gamma_c - \gamma_o) + \frac{g \tan \phi_c}{V_T} \sin \phi_o + \dot{\alpha} \right] - \int_0^t (\gamma_c - \gamma_o) dt \qquad (E1)$$

This equation and the individual components were discussed in the main body of the report. However, when used in the autoland system, constraints were used to limit certain of the terms. These restrictions are:

If $\gamma_c > -0.073$, $\gamma_c = 0$

If $\gamma_c < -0.10472$, $\gamma_c = -0.10472$

If $H > 20.0$, $k_{14} = 1.0$

If $H \leqq 20.0$, $k_{14} = 1.5$

This command was used as indicated in the block diagram, figure 1, to produce a δ_{e_o} which was fed to the elevator.

As previously indicated, flaps and speed commands were keyed to the airplane glide slope. The most satisfactory method for flap control was

If $\gamma_c < 0$, $\delta_f = 0.43633 + 0.08727t$ \qquad (E2)

If $\delta_f \geqq 0.87266$, $\delta_f = 0.87266$

In addition, as indicated in figure 1, the glide slope was used to change speed commands. When γ_c became less than zero, a new speed command was given to the system.

APPENDIX F

AIRPLANE DATA

The airplane used in this study was a typical four-engine jet airliner, with a stretched fuselage, currently in use on civil airlines throughout the world.

Physical Characteristics

Wing span, b, m 43.30

Wing area, S, m^2 . . . . 267.90

Mean aerodynamic chord, $\bar{c}$, m 6.92

Mass, m, kg 90719.4

Inertias:

I_{y_1}, kg-m^2 . . . . 3.896×10^6

I_{y_2}, kg-m^2 . . . . 9.9333×10^6

I_{y_3}, kg-m^2 . . . . 1.3616×10^7

The airplane was powered by four jet engines, each having a maximum thrust of 8.0068×10^4 N.

Aerodynamic Characteristics

Longitudinal aerodynamics, c.g. at 25 percent M.A.C.-

$$C_L = \frac{\partial C_L}{\partial \alpha} \alpha + \frac{\partial C_L}{\partial \delta_f} \left(\delta_f - 0.436332 \right) + 0.7$$

$$C_D = \frac{C_L^2}{7.03\pi} + \frac{\partial C_D}{\partial \delta_f} \left(\delta_f - 0.436332 \right) + 0.037$$

$$\frac{\partial C_L}{\partial \alpha} = 4.87$$

where 0.7 and 0.037 are the values of C_L and C_D for $\alpha = 0.0$.

$$\frac{\partial C_L}{\partial \delta_f} = 0.916732$$

$$\frac{\partial C_D}{\partial \delta_f} = 0.161574$$

The expressions for C_L, C_D, $\frac{\partial C_L}{\partial \delta_f}$, and $\frac{\partial C_D}{\partial \delta_f}$ are for $0.436332 \leq \delta_f \leq 0.872664$.

$$\frac{\partial C_m}{\partial \alpha} = -1.115$$

$$\frac{\partial C_m}{\partial \dot{\alpha}} = -0.241 \text{ sec}$$

$$\frac{\partial C_m}{\partial \dot{\theta}} = -0.707 \text{ sec}$$

$$\frac{\partial C_m}{\partial \delta_e} = -1.017$$

$$\frac{\partial C_m}{\partial \delta_H} = -1.803$$

$$\frac{\partial T}{\partial V} = -260.68 \text{ N-sec-m}^{-1}$$

The flaps were accounted for by varying C_D and C_L as shown in the list of aerodynamic parameters. The lift-curve slopes for the two flap positions were almost the same; therefore, only one value of $\partial C_L / \partial \alpha$ was used.

Lateral aerodynamics, c.g. at 25 percent M.A.C.-

$$\frac{\partial C_Y}{\partial \delta_r} = 0.175$$

$$\frac{\partial C_l}{\partial \delta_r} = 0.114$$

$$\frac{\partial C_n}{\partial \delta_r} = -0.105$$

$$\frac{\partial C_n}{\partial \delta_a} = -0.00344$$

$$\frac{\partial C_l}{\partial \delta_a} = 0.0745$$

$$\frac{\partial C_Y}{\partial \beta} = -0.866$$

$$\frac{\partial C_Y}{\partial \dot{\phi}} = 0.0539 \text{ sec}$$

$$\frac{\partial C_Y}{\partial \dot{\psi}} = 0.0881 \text{ sec}$$

$$\frac{\partial C_l}{\partial \beta} = -0.210$$

$$\frac{\partial C_l}{\partial \dot{\phi}} = -0.111 \text{ sec}$$

$$\frac{\partial C_l}{\partial \dot{\psi}} = 0.0614 \text{ sec}$$

$$\frac{\partial C_n}{\partial \beta} = 0.173$$

$$\frac{\partial C_n}{\partial \dot{\phi}} = -0.0182 \text{ sec}$$

For the spoiler yawing-moment coefficient:

If $\delta_{sp} \leqq -0.34907$, $C_{n_{sp}} = -0.00716\delta_{sp}$

If $-0.34907 < \delta_{sp} < -0.14835$, $C_{n_{sp}} = -0.012319\delta_{sp} - 0.0018275$

If $-0.14835 \leqq \delta_{sp} \leqq 0.14835$, $C_{n_{sp}} = 0.0$

If $0.14835 < \delta_{sp} < 0.34907$, $C_{n_{sp}} = -0.012319\delta_{sp} + 0.0018275$

If $\delta_{sp} \geqq 0.34907$, $C_{n_{sp}} = -0.00716\delta_{sp}$

For the spoiler rolling-moment coefficient:

If $\delta_{sp} \leqq -0.34907$, $C_{l_{sp}} = -0.02544\delta_{sp}$

If $-0.34907 < \delta_{sp} < -0.12217$, $C_{l_{sp}} = -0.04107\delta_{sp} - 0.0049$

If $-0.12217 \leqq \delta_{sp} \leqq 0.12217$, $C_{l_{sp}} = 0.0$

If $0.12217 < \delta_{sp} < 0.34907$, $C_{l_{sp}} = -0.04107\delta_{sp} + 0.0049$

If $\delta_{sp} \geqq 0.34907$, $C_{l_{sp}} = -0.02544\delta_{sp}$

The airplane was simulated by the six-degree-of-freedom equations of rigid body motion. The aerodynamic forces and moments were calculated in stability axes and then transformed to body axes for the computations of airplane motions. At the start of a landing run, the airplane was trimmed for straight and level flight, with the flaps set at 0.43633 rad.

In addition to the airplane parameters already determined, ψ, θ, and ϕ in appendix B, it is also necessary to know the angle of attack α, the angle of sideslip β, their time derivatives, and the flight-path angle γ. The following equations were used to compute these parameters:

$$\alpha = \tan^{-1}\left(\frac{w}{u}\right) \tag{F1}$$

$$\dot{\alpha} = \frac{u\dot{w} - w\dot{u}}{u^2 + w^2} \tag{F2}$$

$$\beta = \tan^{-1}\left(\frac{v}{u}\right) \tag{F3}$$

$$\dot{\beta} = \frac{u\dot{v} - v\dot{u}}{u^2 + v^2} \tag{F4}$$

The usual definition for γ is $\theta - \alpha$; however, this definition is only useful for extremely small roll angles because θ and α are measured in different planes inclined from each other by the roll angle. In this study, the definition adopted for γ is the angle between the velocity vector and a plane parallel to the ground, with γ measured in the z_j coordinate system; thus,

$$\gamma = -\tan^{-1}\left(\dot{z}_3 / \dot{z}_1\right) \tag{F5}$$

and is compatible with the command value of γ that is computed by equations (4), (5), and (11).

REFERENCES

1. Gorham, John A.: Design and Development of the Fail Operative Automatic Landing System for the Lockheed L-1011. SAE Trans., vol. 78, 1969, pp. 1500-1513.

2. Popik, Michael J.: Automated Landing System. Sperry Rand Eng. Rev., vol. 24, no. 2, 1971, pp. 24-31.

3. RTCA Special Committee 117: A New Guidance System for Approach and Landing. Vols. 1 and 2. Doc. DO-148, Radio Tech. Comm. Aeronaut., Dec. 18, 1970.

4. Anon.: National Plan for Development of the Microwave Landing System. FAA, DOD, and NASA, July 1971.

5. Adams, James J.: An Analog Study of an Airborne Automatic Landing-Approach System. NASA TN D-105, 1959.

6. Erzberger, Heinz; and Lee, Homer Q.: Terminal-Area Guidance Algorithms for Automated Air-Traffic Control. NASA TN D-6733, 1972.

7. Cherry, George W.; MacKinnon, Duncan; and DeWolf, Barton: A New Approach and Landing System: Help for Our Troubled Terminal Areas. R-654, Charles Stark Draper Lab., Massachusetts Inst. Technology, Mar. 1970.

8. Anon.: Engineering and Development Program Plan – All Weather Landing. FAA-ED-07-3, Oct. 1972. (Available from DDC as AD 754 264.)

9. Niessen, Frank R.: A Low-Cost Inertial Smoothing System for Landing Approach Guidance. NASA TN D-7271, 1973.

TABLE I.- VALUES OF THRUST USED FOR SPEED CONTROL SYSTEM

Thrust, T	Time, t
5.24890151×10^3	0.25
1.10315896×10^4	.5
1.69032421×10^4	.75
2.44652189×10^4	1.0
3.33616621×10^4	1.25
4.09236389×10^4	1.4
4.67063270×10^4	1.5
5.56027702×10^4	1.625
7.11715458×10^4	1.75
9.45247093×10^4	1.875
1.13429651×10^5	2.0
1.25217438×10^5	2.125
1.31222538×10^5	2.25
1.38784514×10^5	2.5
1.44567202×10^5	2.75
1.49015424×10^5	3.0
1.53241235×10^5	3.25
1.56577401×10^5	3.5
1.60047014×10^5	3.75
1.62360089×10^5	4.0
1.64584200×10^5	4.25
1.66808311×10^5	4.5
1.69032421×10^5	4.75
1.71212050×10^5	5.0
1.73391679×10^5	5.25
1.74592698×10^5	5.5
1.76816809×10^5	5.75
1.77928865×10^5	5.9

TABLE II.- INITIAL AND TOUCHDOWN CONDITIONS

	Initial condition				Touchdown condition									
					Lateral					Vertical				
Case	ζ_1	ζ_2	ψ_i	H	t, sec	ϕ	ψ	ζ_2	k_4	k_1	ζ_1	γ	θ	w_{z_j}
1	-6000	-2000	$\pi/2$	540	101.6	-2.45×10^{-3}	5.0×10^{-3}	-0.60	3.0	1.483	48.6	-1.13×10^{-2}	1.17×10^{-2}	1.558
2			$\pi/4$	540	90.6	-1.33×10^{-3}	9.47×10^{-4}	-.15	4.8	1.483	124.7	-1.73×10^{-3}	3.48×10^{-3}	.345
3			0	540	90.2	-1.98×10^{-3}	1.43×10^{-3}	-.23	4.8	1.483	121.0	-1.70×10^{-3}	3.66×10^{-3}	.355
4			$-\pi/6$	540	93.5	-5.41×10^{-3}	2.85×10^{-3}	-.41	4.8	1.483	62.5	-6.20×10^{-3}	8.32×10^{-3}	.983
5		2000	$-\pi/2$	540	102.6	-1.65×10^{-4}	-4.18×10^{-3}	0.92	3.0	1.524	46.1	-1.23×10^{-2}	1.17×10^{-2}	1.626
6			$-\pi/4$	540	90.5	2.70×10^{-3}	-1.92×10^{-3}	.33	4.8	1.524	133.7	-2.44×10^{-3}	2.79×10^{-3}	.346
7			0	540	90.2	3.89×10^{-3}	-2.66×10^{-3}	.46	4.8	1.524	130.2	-2.41×10^{-3}	3.02×10^{-2}	.327
8			$\pi/6$	540	93.7	8.49×10^{-3}	-4.51×10^{-3}	.73	4.8	1.524	68.1	-5.97×10^{-3}	8.62×10^{-3}	.986
9		-4000	$\pi/2$	540	121.4	8.25×10^{-4}	3.56×10^{-3}	-0.91	3.0	1.483	32.4	-2.42×10^{-2}	6.29×10^{-3}	2.101
10			$\pi/4$	540	110.0	-5.58×10^{-3}	1.53×10^{-3}	-.14	4.8	1.483	34.9	-1.88×10^{-2}	6.82×10^{-3}	1.764
11			0	540	111.8	-6.93×10^{-3}	2.08×10^{-3}	-.21	4.8	1.483	35.0	-2.0×10^{-2}	1.26×10^{-2}	2.219
12		4000	$-\pi/2$	540	121.8	-1.70×10^{-3}	-2.23×10^{-3}	0.82	3.0	1.524	31.4	-2.45×10^{-2}	5.68×10^{-3}	2.085
13			$-\pi/4$	540	109.9	8.01×10^{-3}	-3.0×10^{-3}	.44	4.8	1.524	37.5	-1.81×10^{-2}	8.20×10^{-3}	1.805
14			0	540	112.4	8.93×10^{-3}	-3.50×10^{-3}	.53	4.8	1.524	37.5	-1.95×10^{-2}	1.74×10^{-2}	2.475
15	-4000	-4000	$\pi/2$	540	92.6	-6.77×10^{-4}	-1.74×10^{-3}	0.64	3.0	1.748	49.4	-9.17×10^{-3}	8.63×10^{-3}	1.214
16			$\pi/4$	540	88.1	-7.14×10^{-3}	7.43×10^{-3}	-1.30	4.8	[a]1.748; 1.524	74.5	-5.26×10^{-3}	6.73×10^{-3}	.810
17			0	540	88.7	5.15×10^{-3}	1.35×10^{-2}	-4.49	4.8	[a]1.748; 1.60	6.6	-1.02×10^{-2}	1.47×10^{-2}	1.710
18		4000	$-\pi/2$	540	92.9	1.95×10^{-3}	-9.18×10^{-4}	0.03	3.0	1.80	50.1	-9.46×10^{-3}	9.05×10^{-3}	1.261
19			$-\pi/4$	540	88.2	1.15×10^{-2}	-9.79×10^{-3}	1.71	4.8	[a]1.799; 1.585	93.9	-4.95×10^{-3}	6.49×10^{-3}	.767
20			0	540	88.8	-2.02×10^{-2}	-1.54×10^{-2}	.55	4.8	[a]1.799; 1.671	-39.3	-2.25×10^{-2}	1.51×10^{-2}	2.638
21	-3000	-4000	$\pi/2$	540	80.9	-2.61×10^{-2}	9.5×10^{-3}	1.39	3.0	2.0	192.0	-8.66×10^{-3}	2.37×10^{-5}	0.563
22			$\pi/4$	540	77.2	-1.1×10^{-2}	2.59×10^{-2}	-5.71	4.8	[a]2.0; 1.720	221.7	-1.32×10^{-2}	-7.20×10^{-4}	.819
23			0	540	82.6	3.28×10^{-2}	2.39×10^{-2}	-7.38	4.8	[a]2.0; 1.89	367.2	-1.28×10^{-2}	3.85×10^{-2}	3.165
24		4000	$-\pi/2$	540	81.1	2.17×10^{-2}	-1.16×10^{-2}	0.15	3.0	2.1	188.8	-8.42×10^{-3}	3.62×10^{-5}	0.551
25			$-\pi/4$	540	77.3	8.10×10^{-3}	-3.14×10^{-2}	7.64	4.8	[a]2.07; 1.79	219.5	-1.32×10^{-2}	-1.40×10^{-3}	.777
26			0	540	79.1	2.16×10^{-1}	1.15×10^{-1}	-25.22	4.8	[a]2.067; 1.973	71.3	-9.72×10^{-3}	3.17×10^{-2}	2.516
27		-4000	$\pi/2$	528	79.4	-2.47×10^{-2}	4.73×10^{-3}	2.23	3.0	2.0	26.6	-3.06×10^{-3}	1.37×10^{-2}	1.135
28			$\pi/2$	200	81.1	-3.02×10^{-2}	1.10×10^{-2}	.92	3.0	2.0	46.7	-1.06×10^{-2}	1.62×10^{-2}	1.802
29		4000	$-\pi/2$	528	81.8	7.35×10^{-3}	-2.22×10^{-3}	-0.31	3.0	2.07	169.3	-4.83×10^{-3}	-3.67×10^{-3}	0.079
30			$-\pi/2$	200	81.6	2.23×10^{-2}	-1.19×10^{-2}	.88	3.0	2.07	56.5	-9.55×10^{-3}	1.63×10^{-2}	1.731
[b]31	-6000	-4000	$\pi/2$	540	110.0	-6.41×10^{-3}	2.42×10^{-3}	0.56	4.0	1.42	38.0	-1.73×10^{-2}	1.01×10^{-2}	1.880
[b]32			0	540	104.7	-5.51×10^{-2}	5.49×10^{-2}	-15.05	4.0	1.65	100.8	-1.45×10^{-2}	1.60×10^{-2}	2.044
[c]33	-3000	-4000	$\pi/2$	200	77.8	-2.72×10^{-3}	4.45×10^{-2}	2.94	3.0	2.00	128.9	-1.6×10^{-2}	7.11×10^{-3}	1.610
[d]34			0	540	83.4	-2.14×10^{-2}	3.16×10^{-2}	4.71	4.8	[a]2.00; 1.89	464.8	-7.54×10^{-3}	1.342×10^{-3}	.580

[a]Second value of k_1 is new k_1 introduced at k_1 switch (see fig. 7(a)).

[b]Cases 31 and 32 use the combined turn algorithm.

[c]Flap and speed change commands put in when $\gamma_c = 0$.

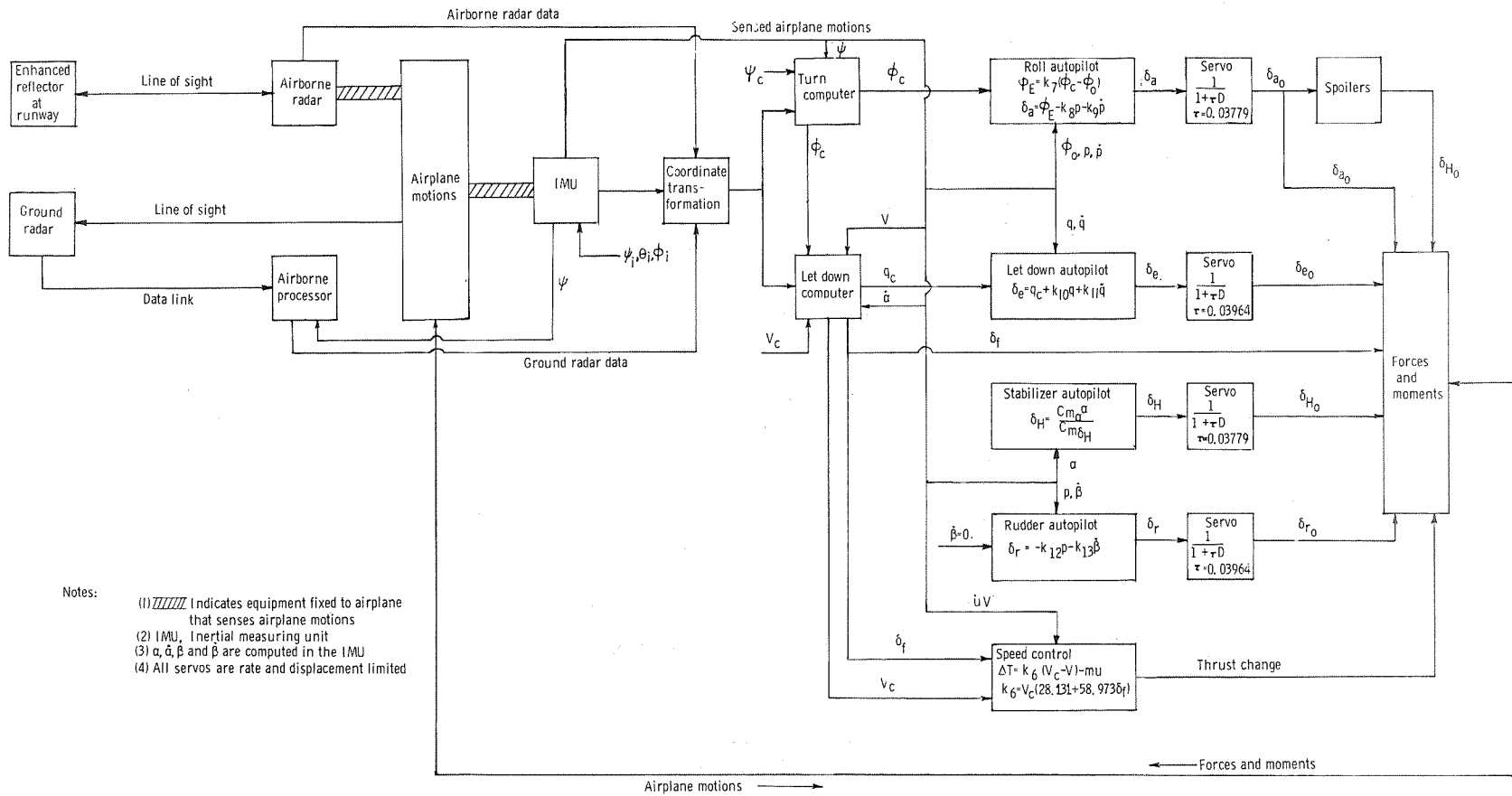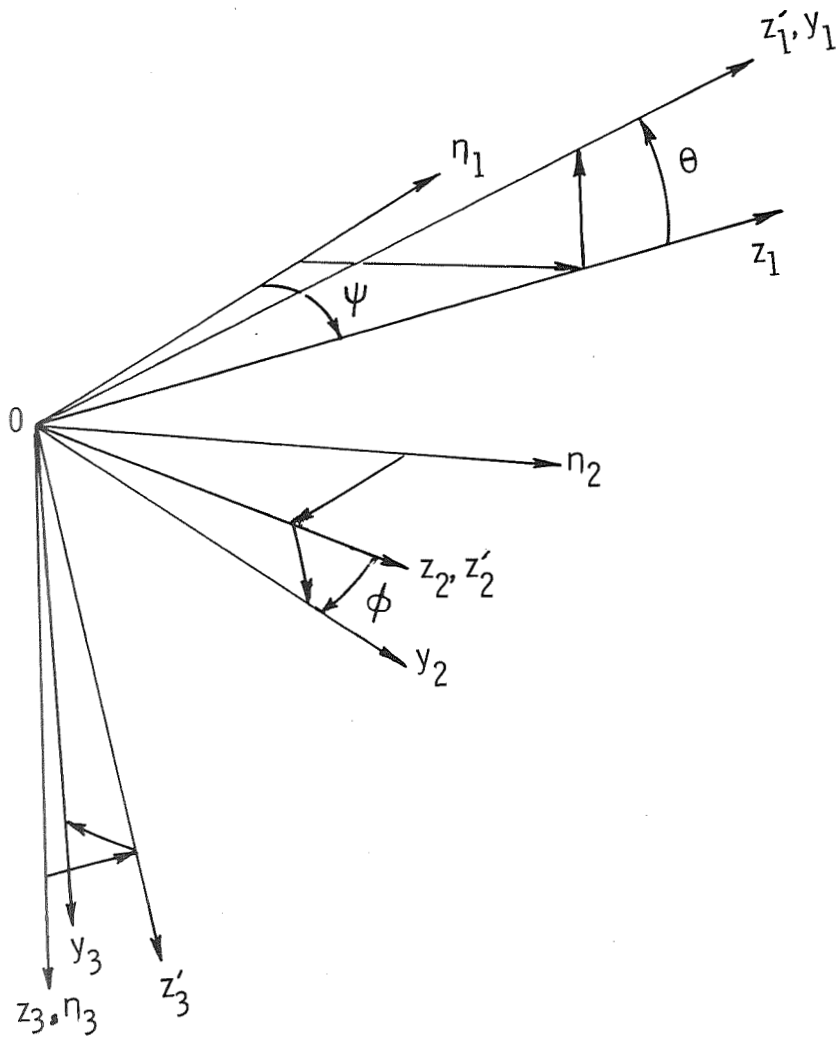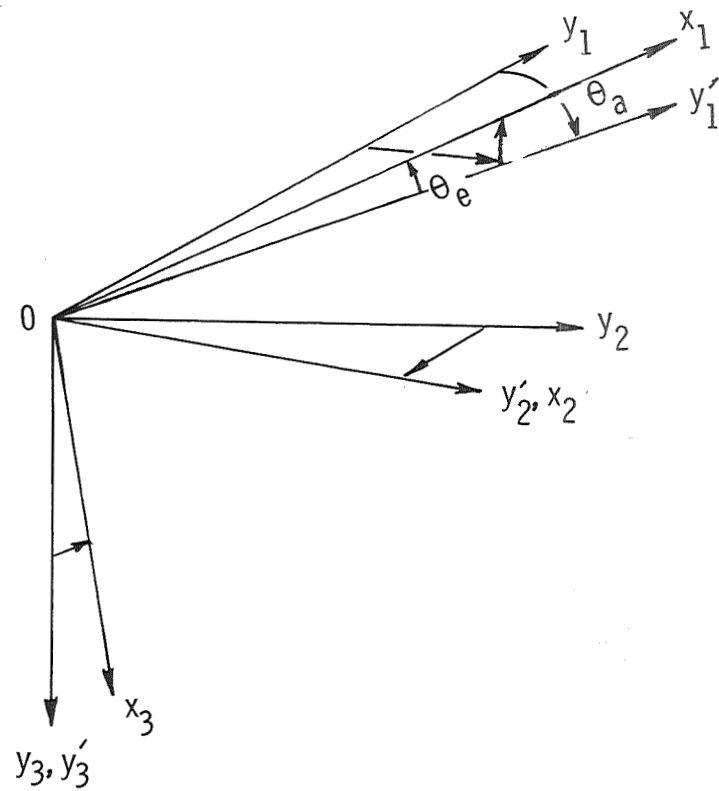[d]Same as case 23 except flare algorithm has been modified.

Figure 1.- Block diagram of the automatic landing system.

(a) Inertial, quasi inertial, and airplane coordinates.

(b) Radar and airplane coordinates.

Figure 2.- Coordinate systems used in study. (A prime on a quantity indicates an intermediate axis.)

Notes

1) Runway coordinates are centered at touchdown point; positive directions shown at right

2) Airplane inertial coordinates are || to runway coordinates but centered in airplane

3) The z_i coordinates are centered in the airplane and rotated away from the airplane inertial coordinates by the Euler angle ψ, the heading angle of the airplane. The following sketch shows these relationships:
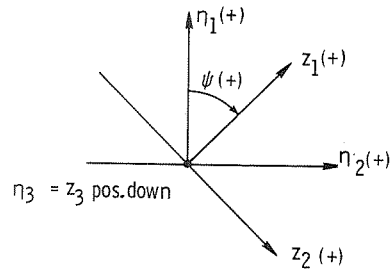
4) For the runway $\psi = \psi_r = 0$

5) The η_1, η_2 plane coincides with the z_1, z_2 plane
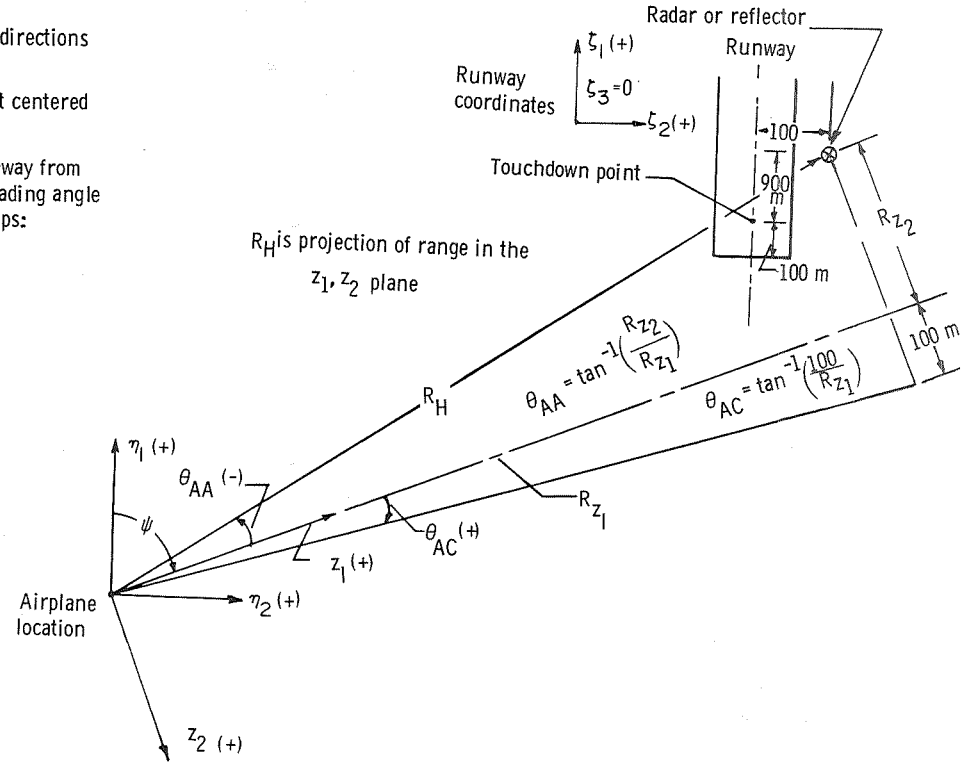
Figure 3.- Geometry used for the turn computer.
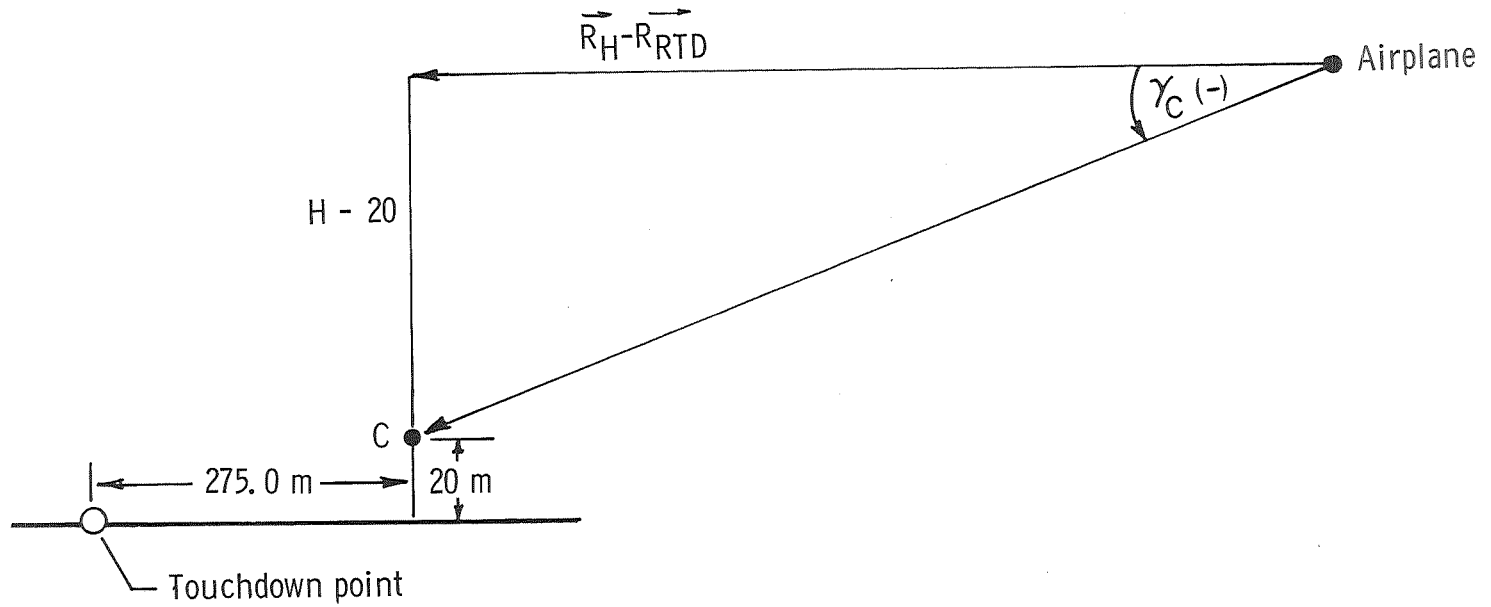
Figure 4.- Geometry used for letdown computer.

Autoland system

Typical ILS path

Runway center line extended

+4000m

1220m

Radar or reflector

-4000m

Runway center line extended

Runway

3000m

Touchdown point

540m

-6000m

-22800m
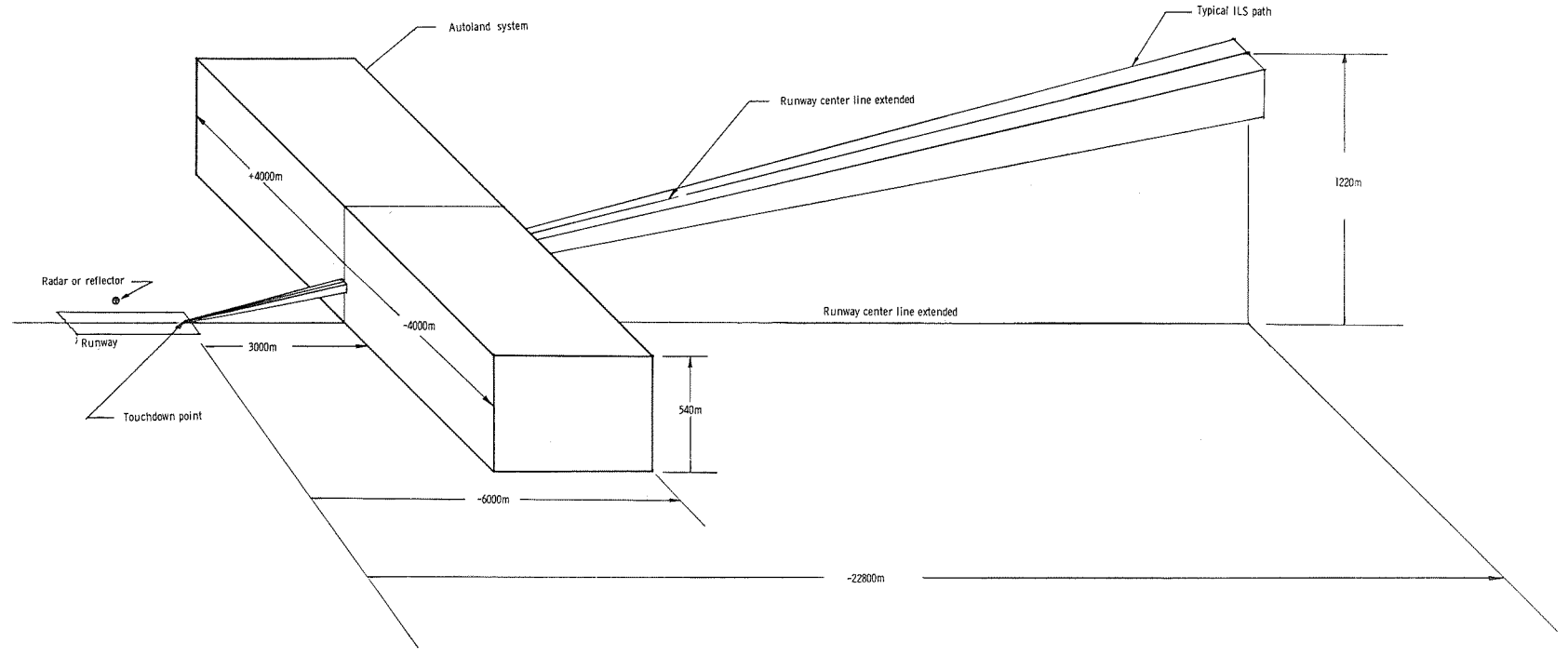
Note: Vertical scale and runway width scale (4) times larger than basic scale. All distances in runway coordinates

Figure 5.- Comparison of autoland and current ILS zones of operation.
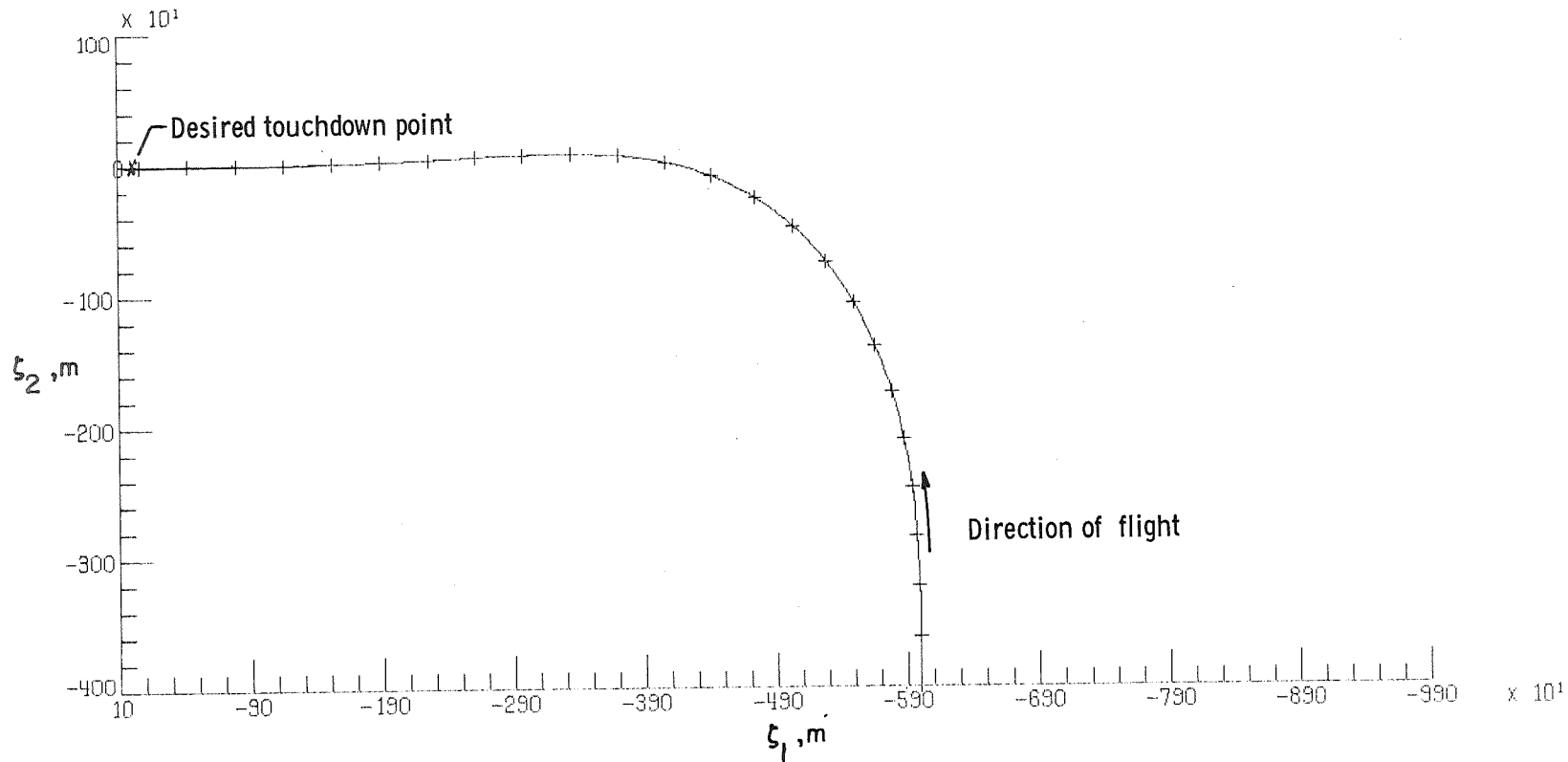
(a) Ground track.

Figure 6.- Airplane and system response for initial condition $\zeta_1 = -6000$ m, $\zeta_2 = -4000$ m, $H = 540$ m, $\psi_i = \frac{\pi}{2}$ (case 9 of table II). Tick marks represent 5-sec intervals.
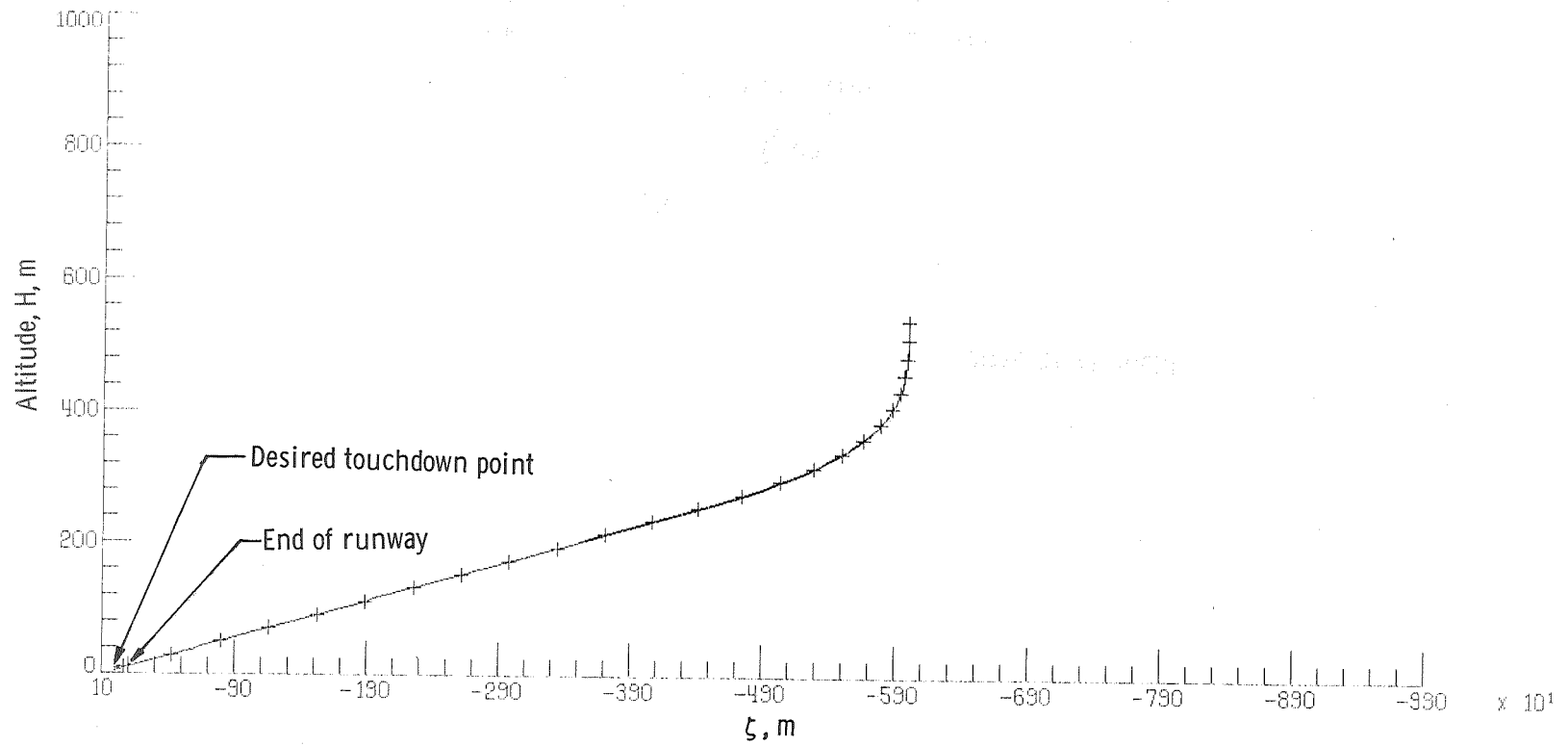
(b) Altitude track with respect to the ground.

Figure 6.- Continued.
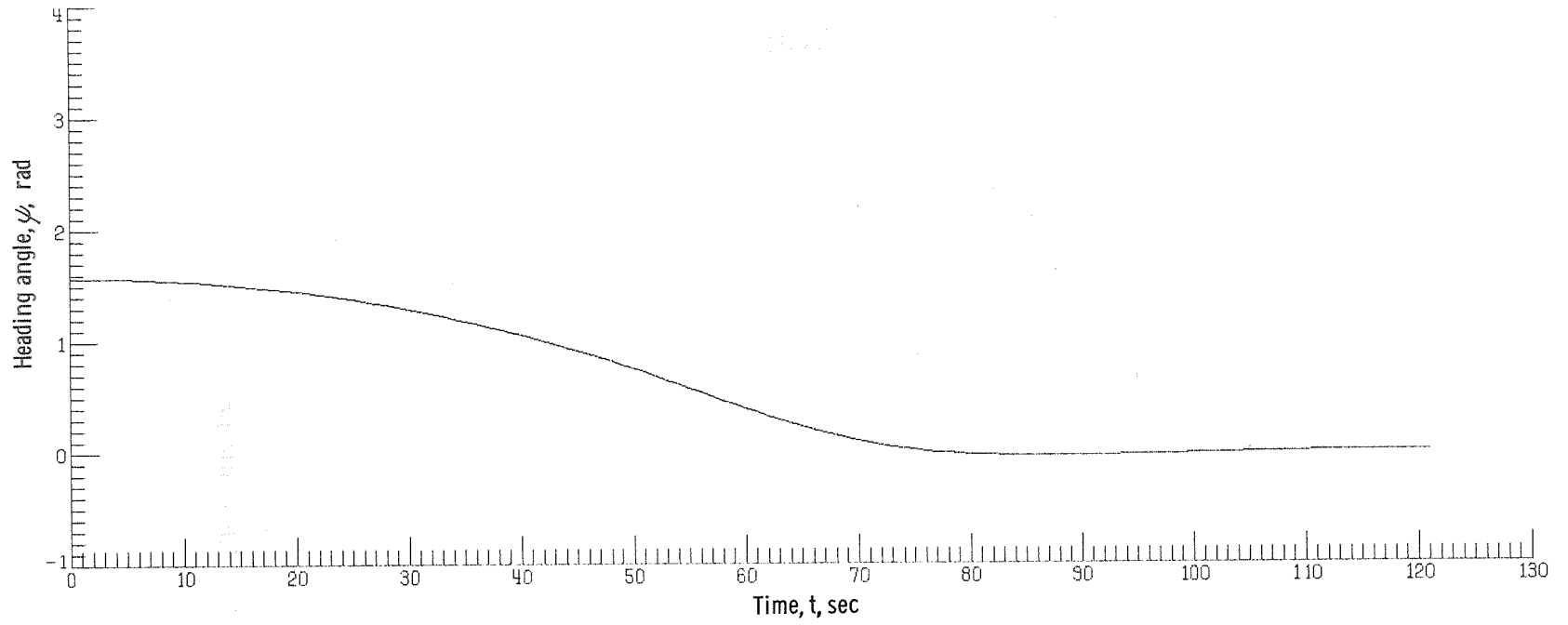
(c) Heading angle.

Figure 6.- Continued.
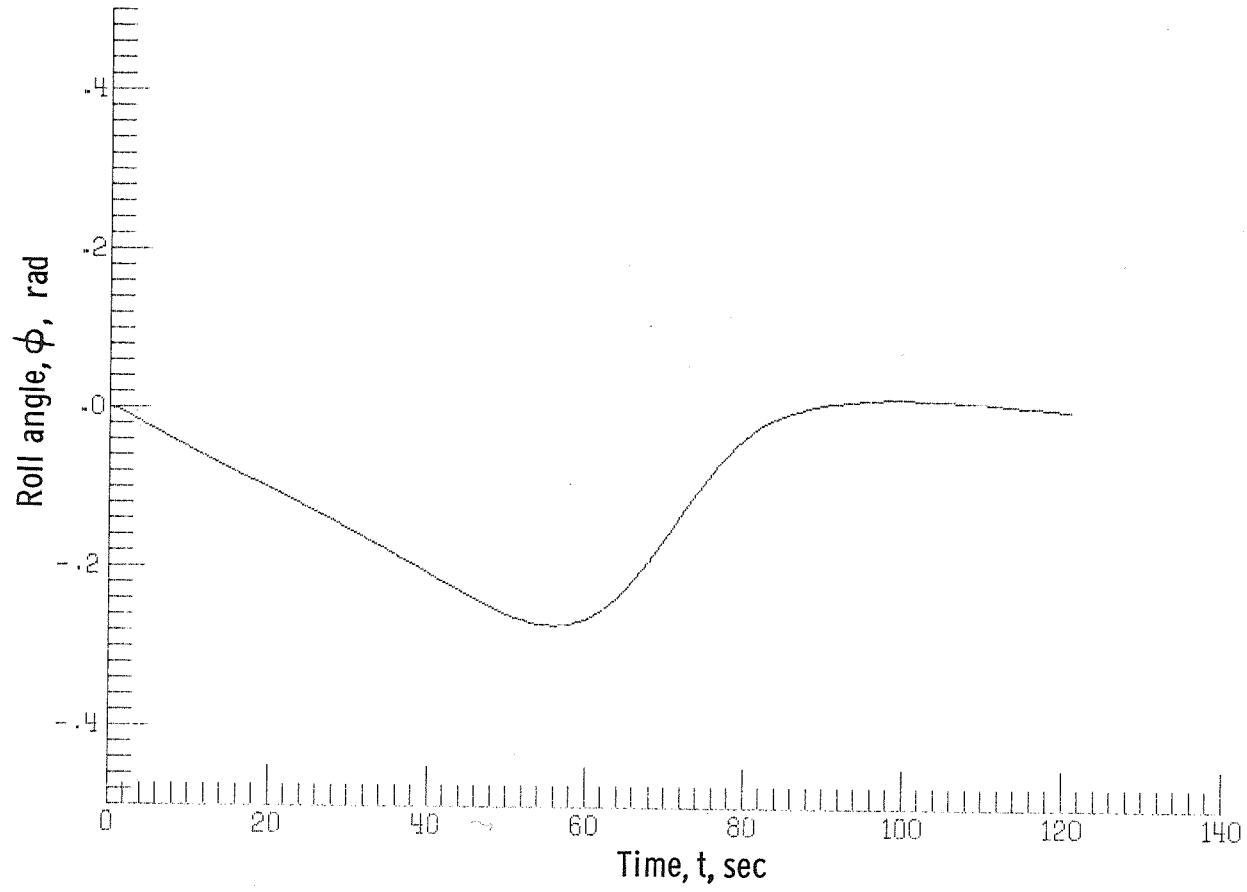
(d) Roll angle.

Figure 6.- Continued.
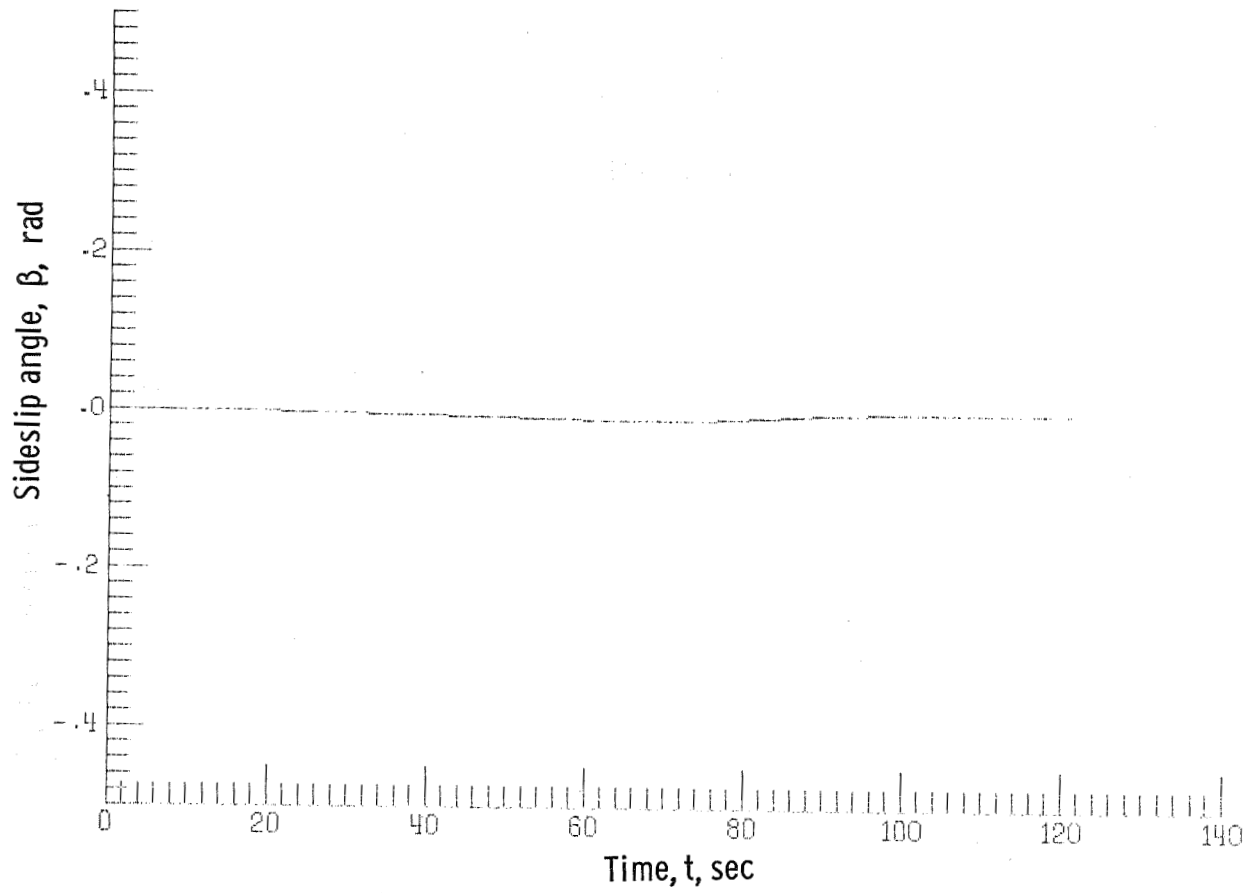
(e) Sideslip angle.

Figure 6.- Continued.
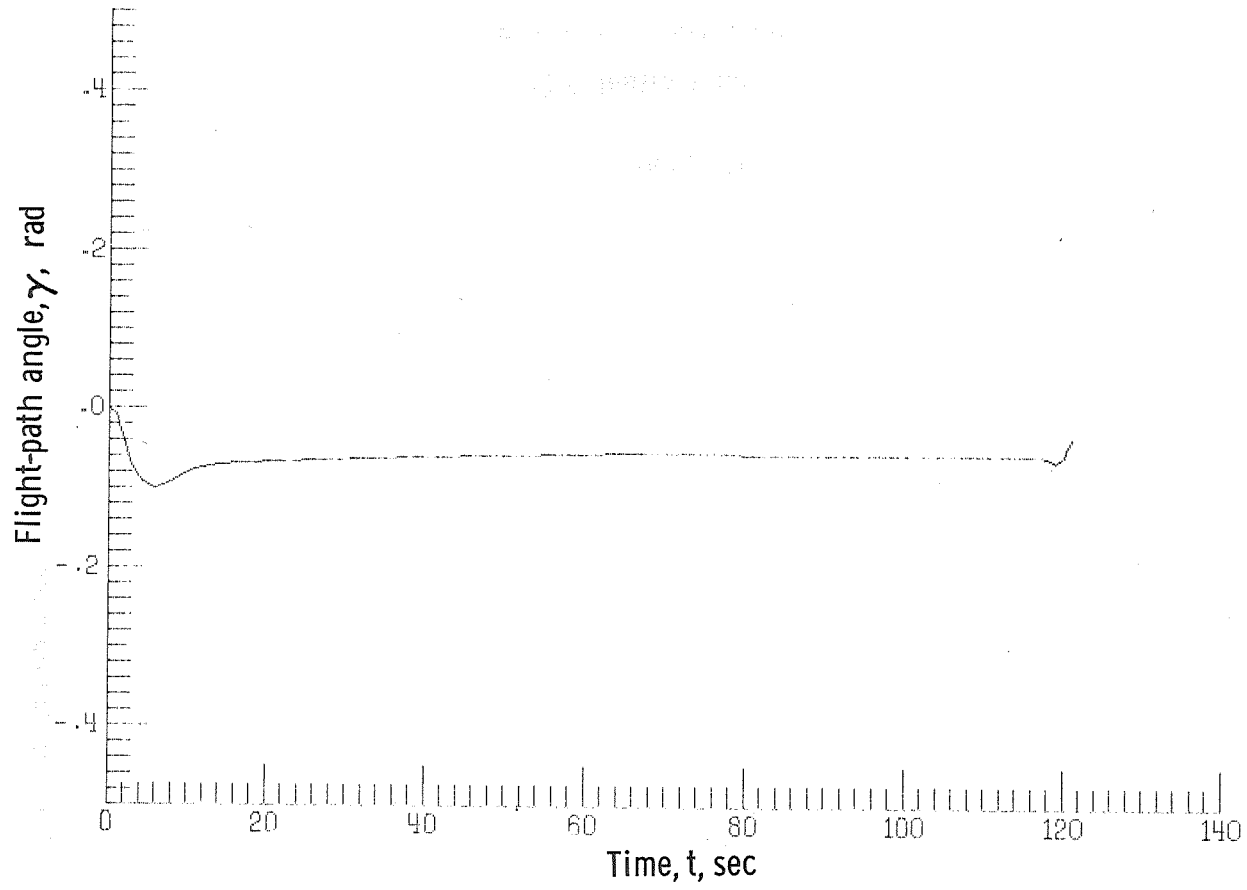
(f) Flight-path angle.

Figure 6.- Continued.
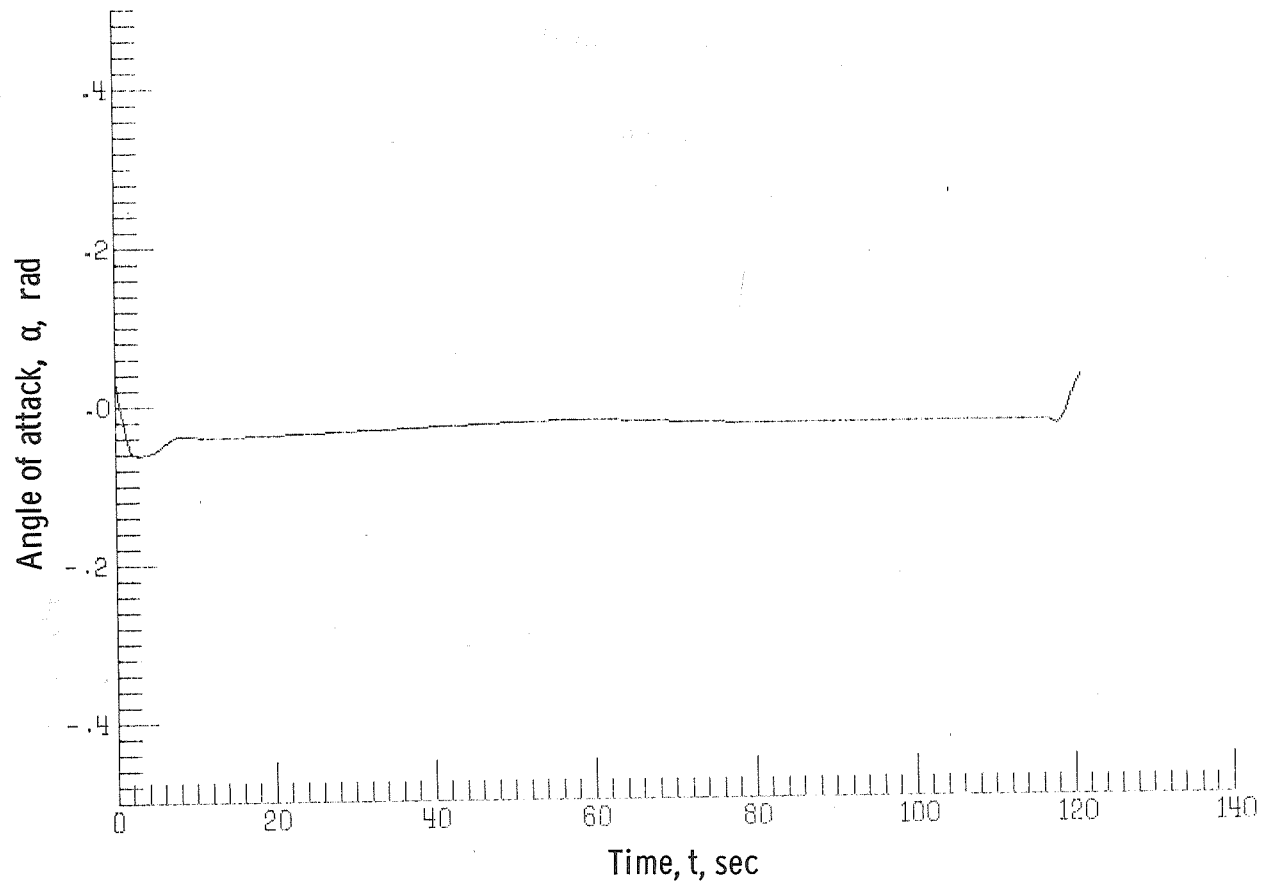
(g) Angle of attack.

Figure 6.- Continued.
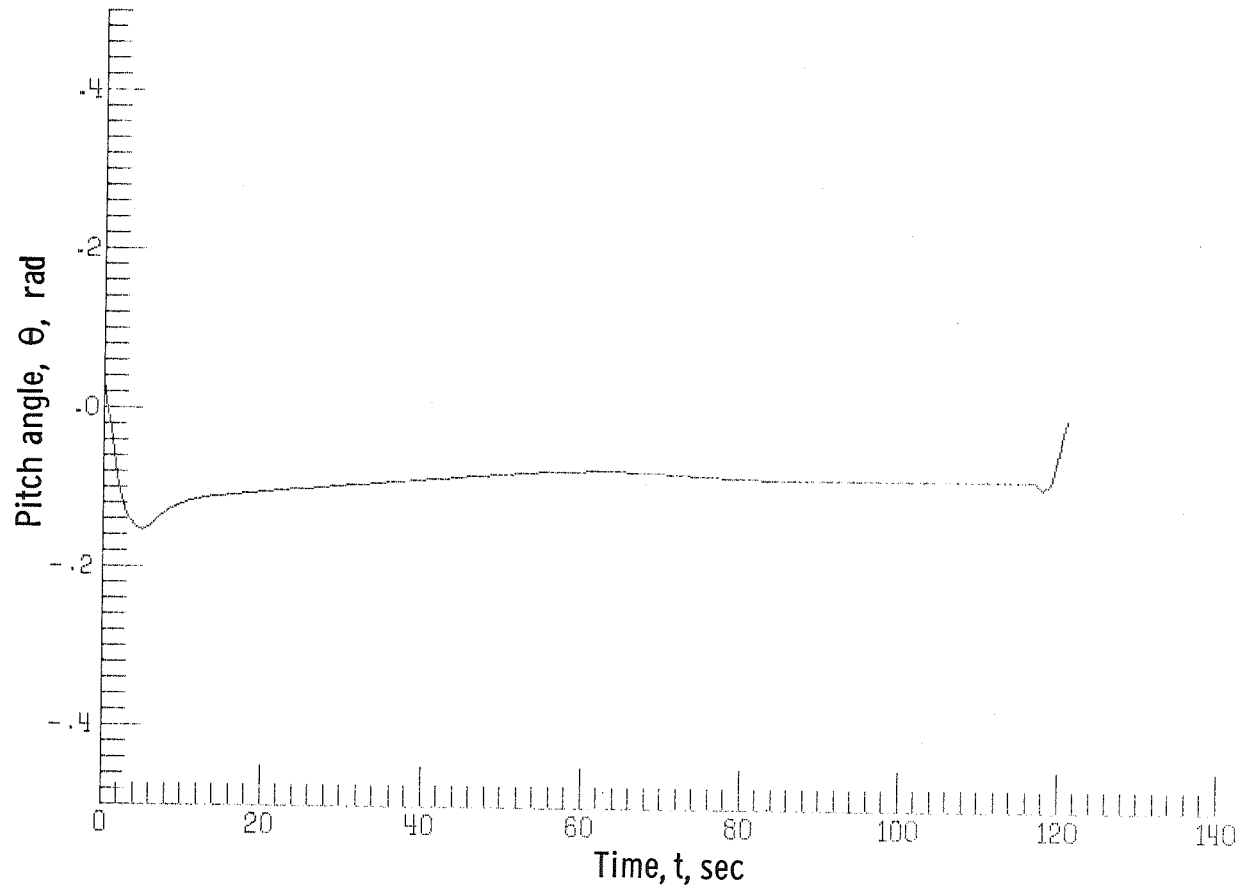
(h) Pitch angle.

Figure 6.- Concluded.
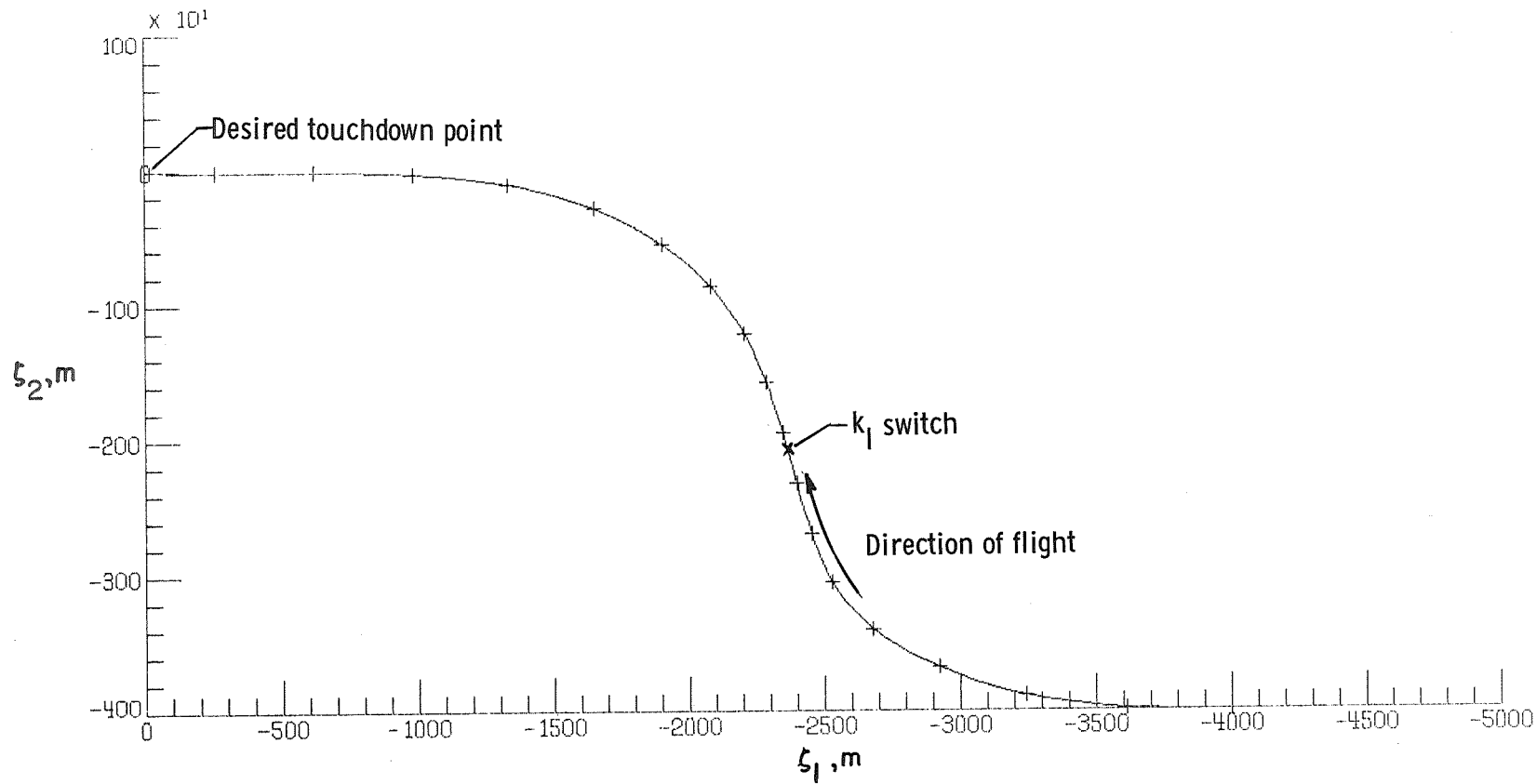
(a) Ground track.

Figure 7.- Airplane and system response for the initial condition ζ_1 = -4000 m, ζ_2 = -4000 m, H = 540 m, ψ_i = 0.0 (case 17 of table II). Tick marks indicate 5-sec intervals.
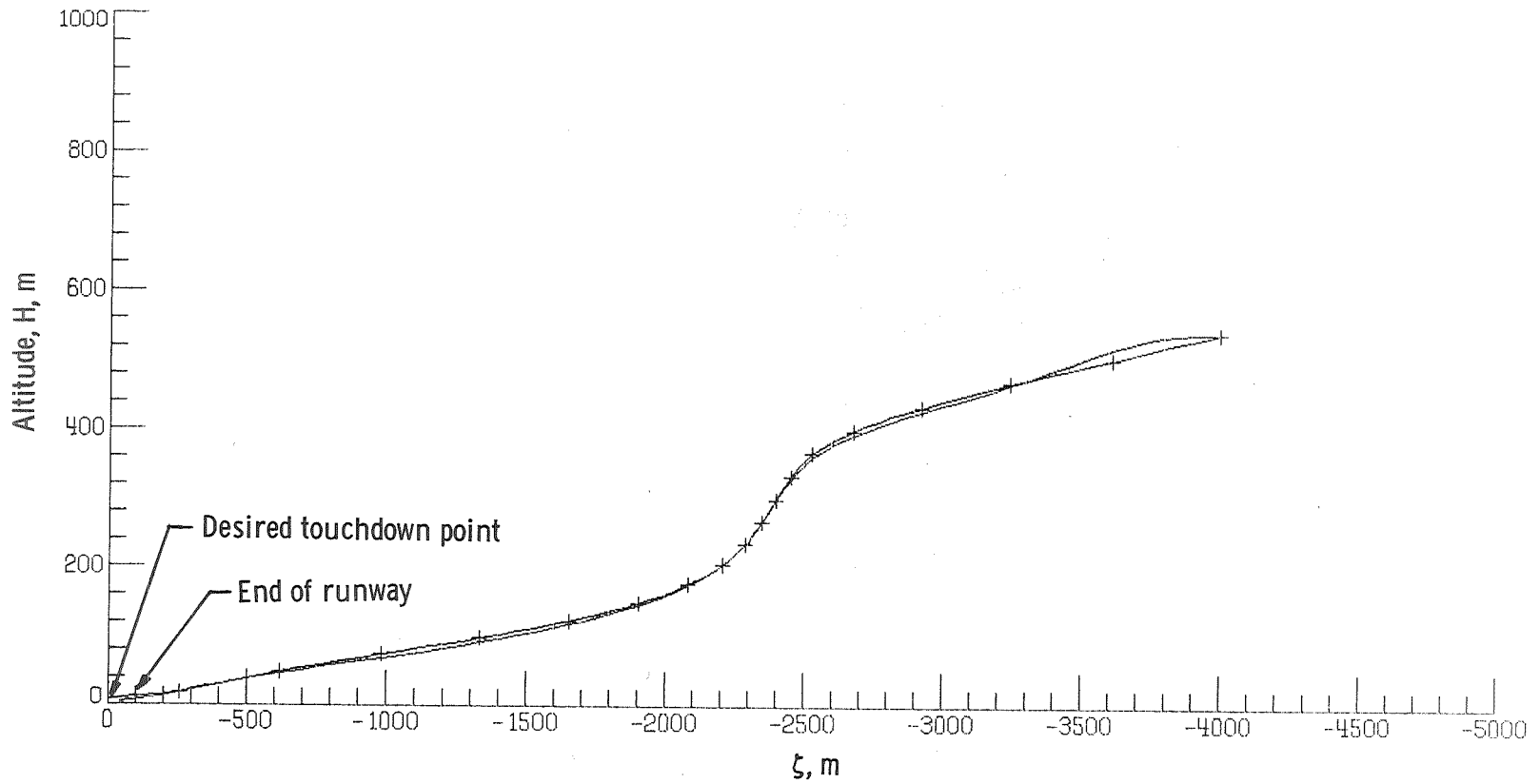
(b) Altitude track with respect to the ground.

Figure 7.- Continued.
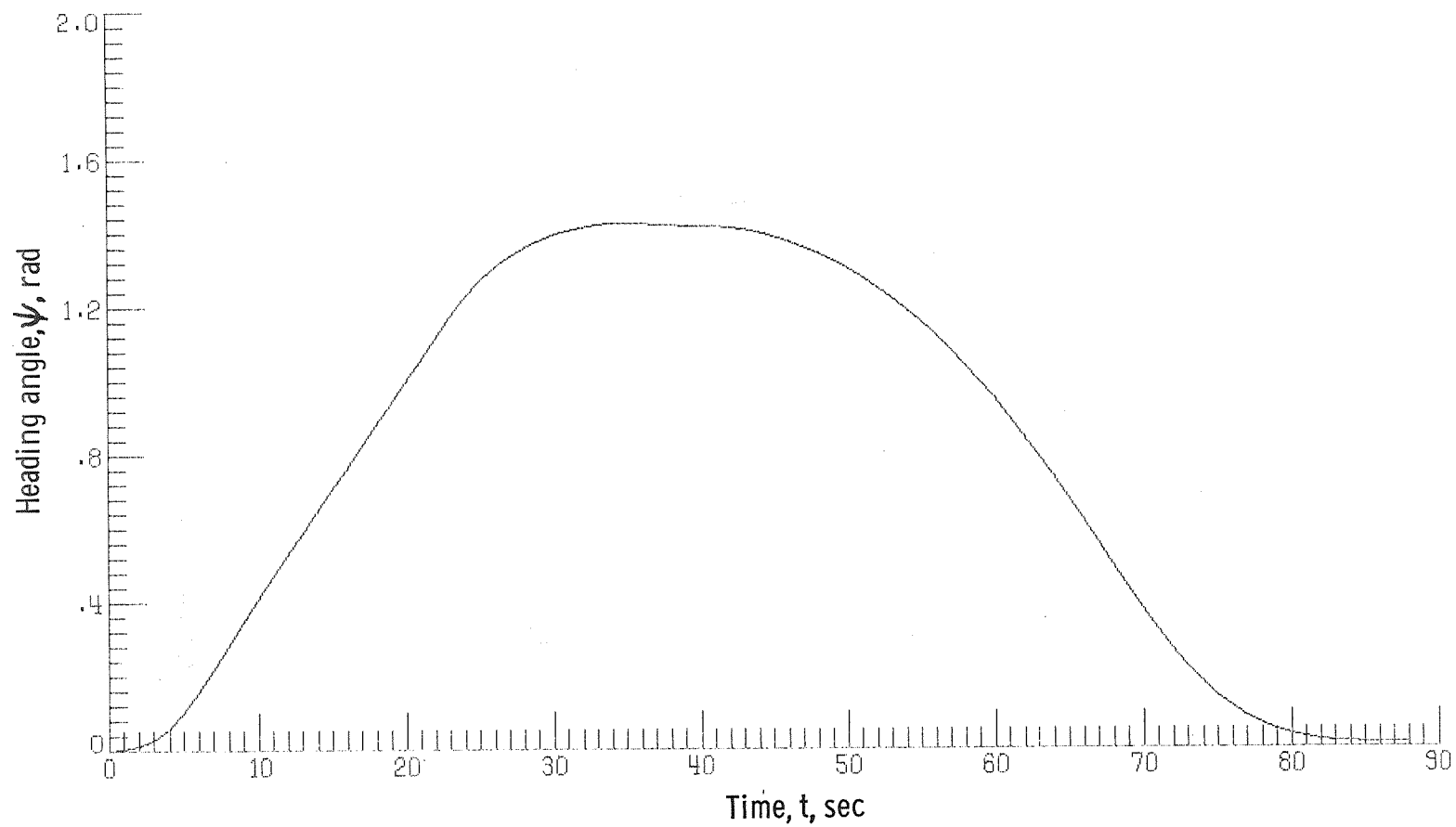
(c) Heading angle.

Figure 7.- Continued.
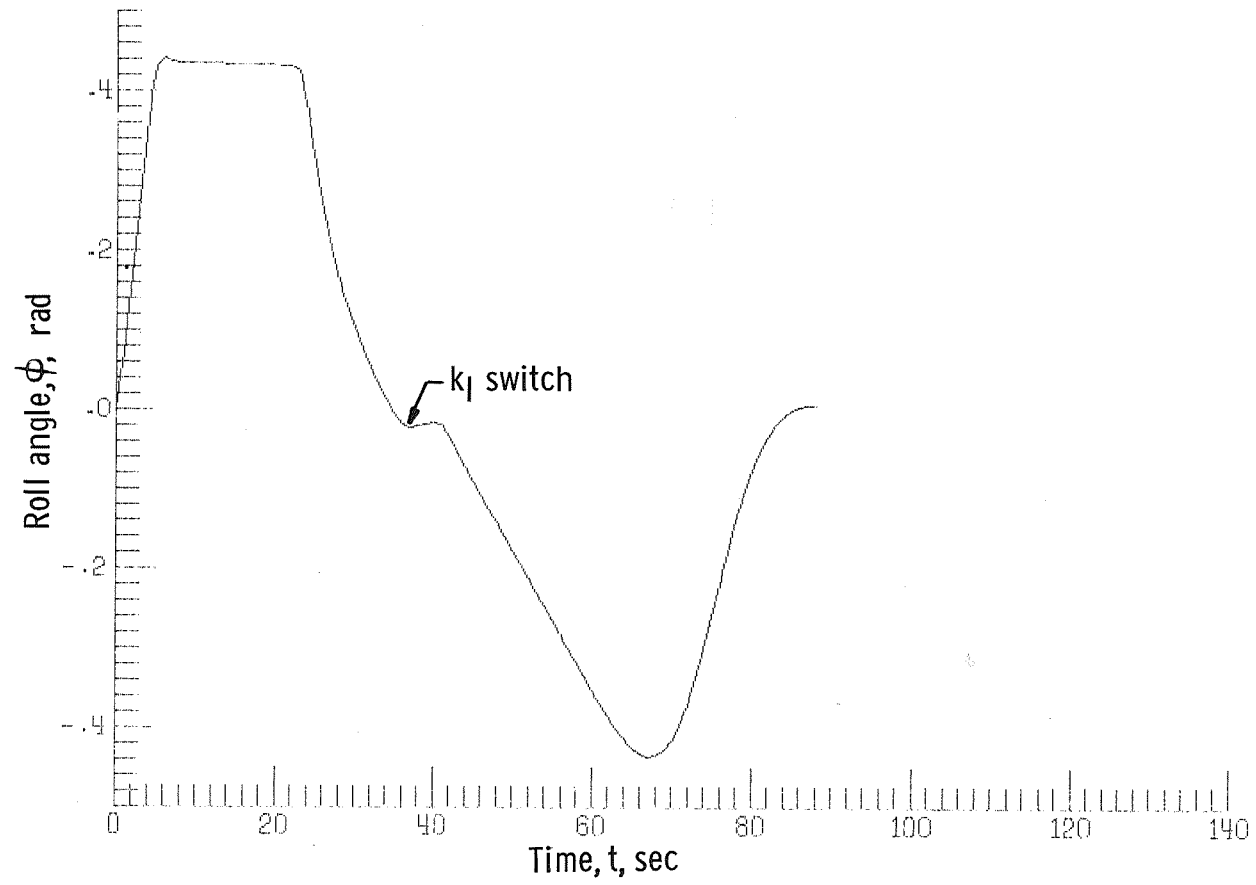
(d) Roll angle.

Figure 7.- Continued.
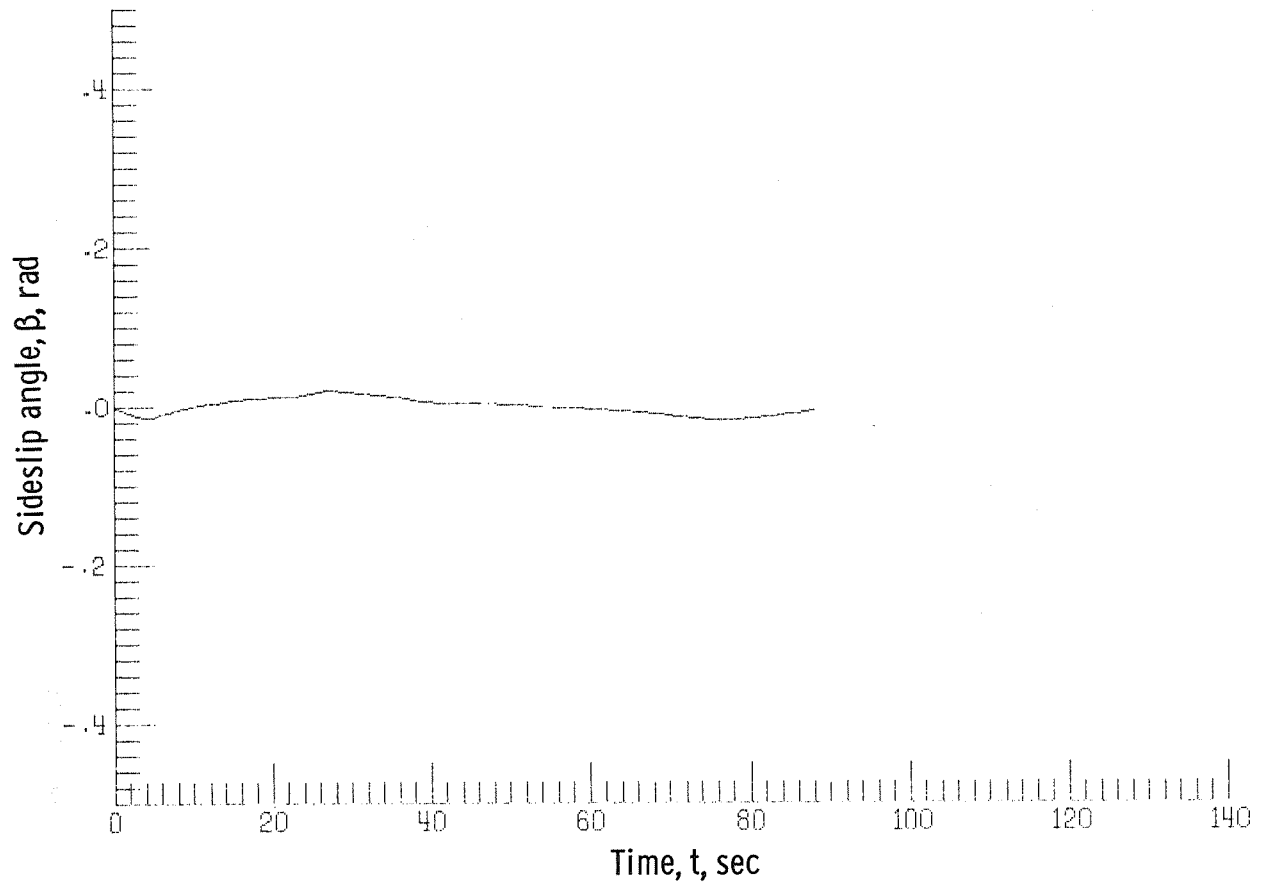
(e) Sideslip angle.

Figure 7.- Continued.
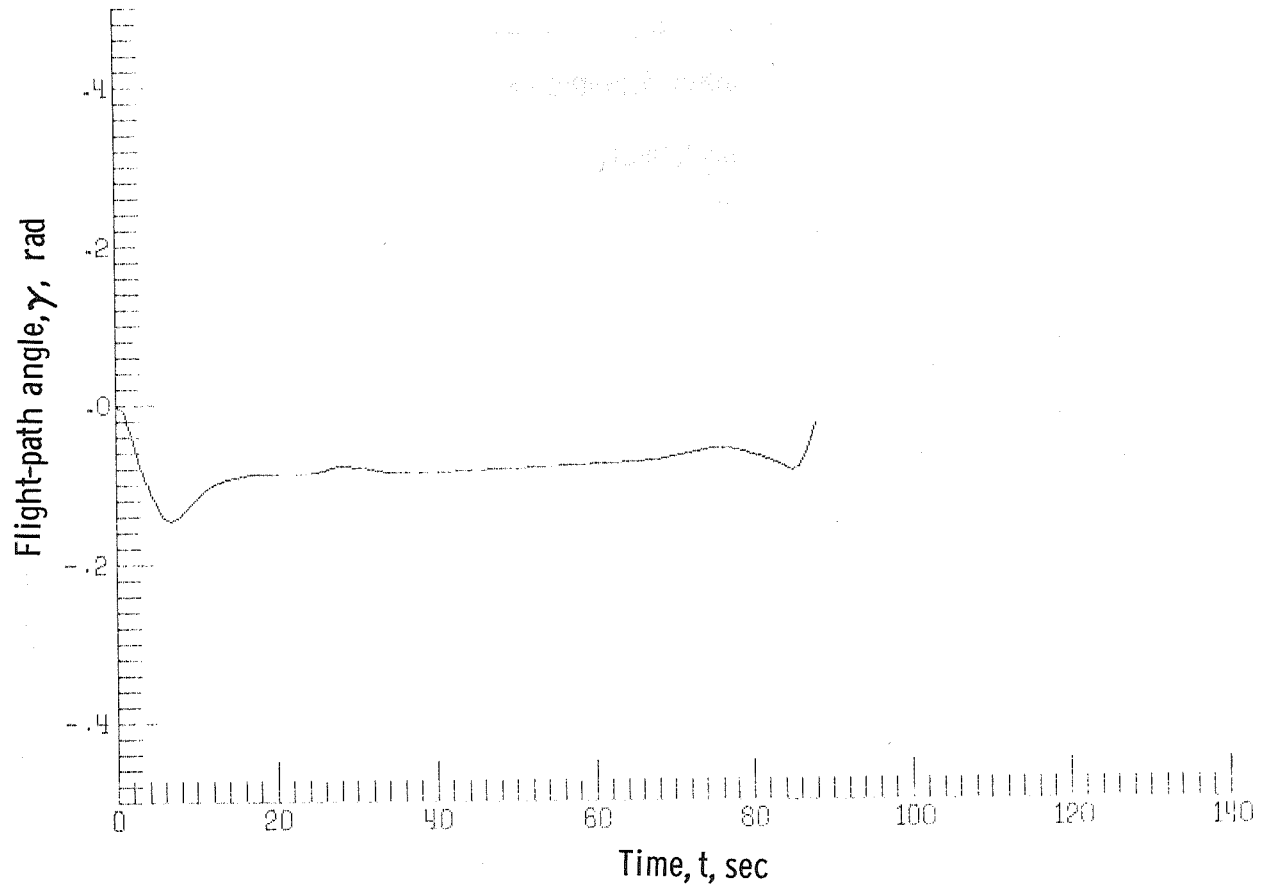
(f) Flight-path angle.

Figure 7.- Continued.
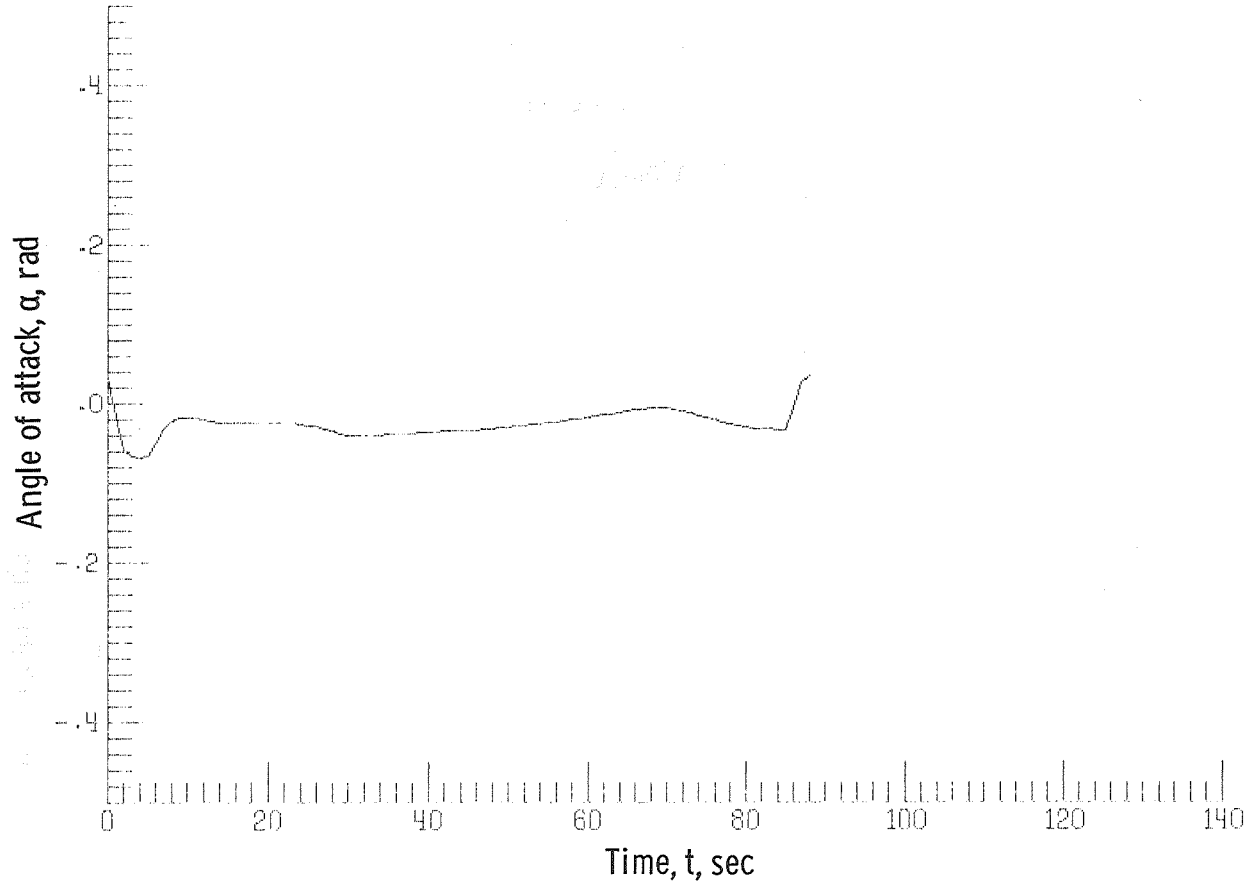
(g) Angle of attack.

Figure 7.- Continued.
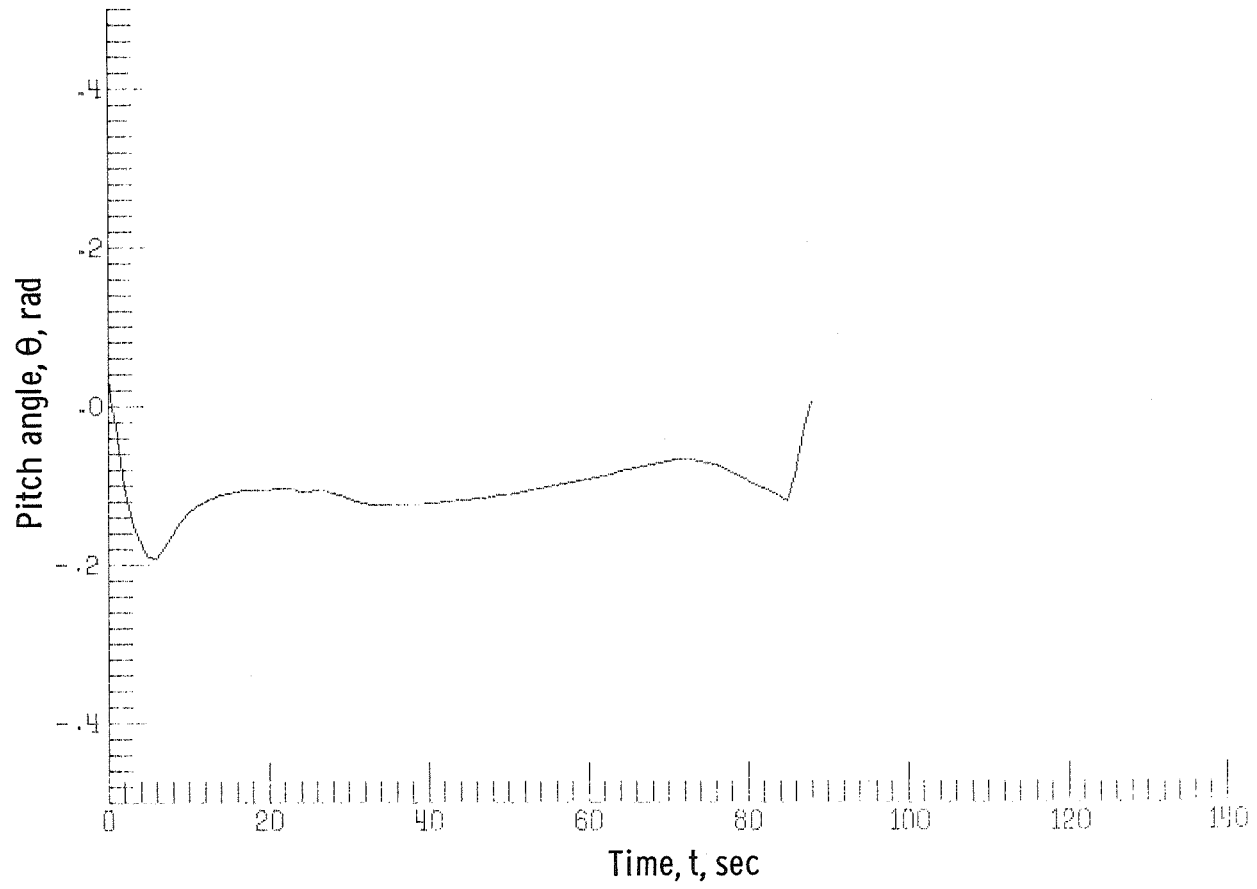
(h) Pitch angle.

Figure 7.- Concluded.
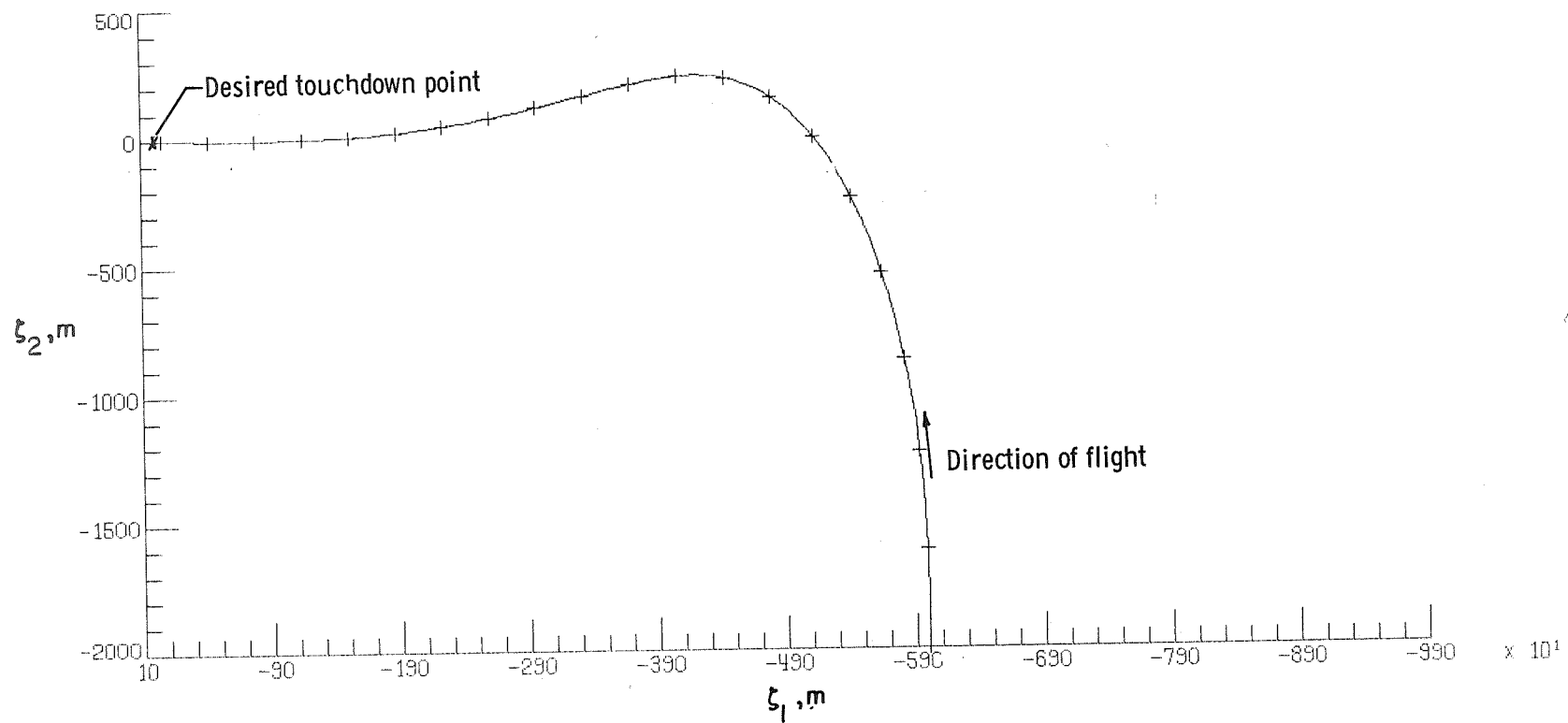
Figure 8.- Ground track for the initial condition $\zeta_1 = -6000$ m, $\zeta_2 = -2000$ m, H = 540 m, $\psi_i = \frac{\pi}{2}$ (case 1 of table II). Tick marks indicate 5-sec intervals.
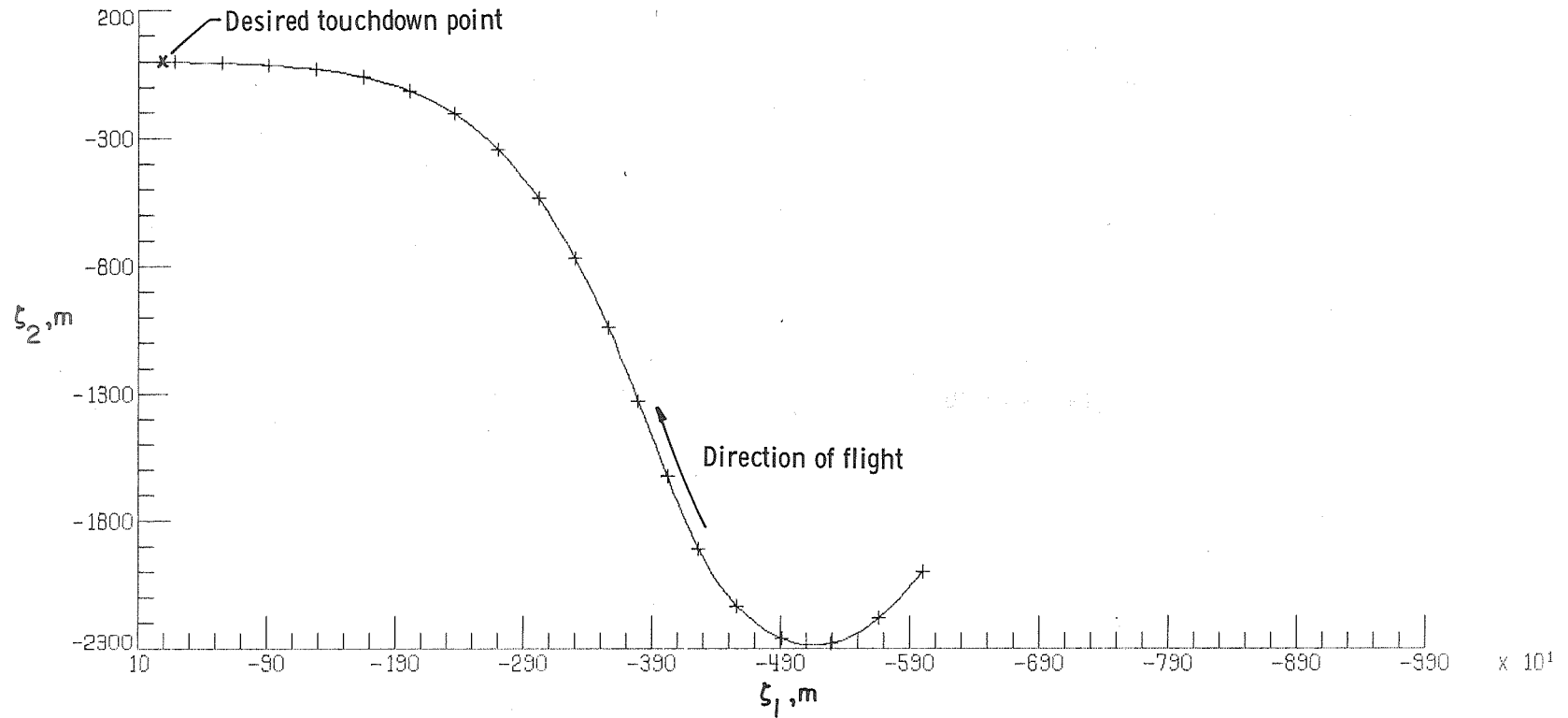
Figure 9.- Ground track for the initial condition $\zeta_1 = -6000$ m, $\zeta_2 = -2000$ m, H = 540 m, $\psi_i = -\frac{\pi}{6}$ (case 4 of table II). Tick marks indicate 5-sec intervals.
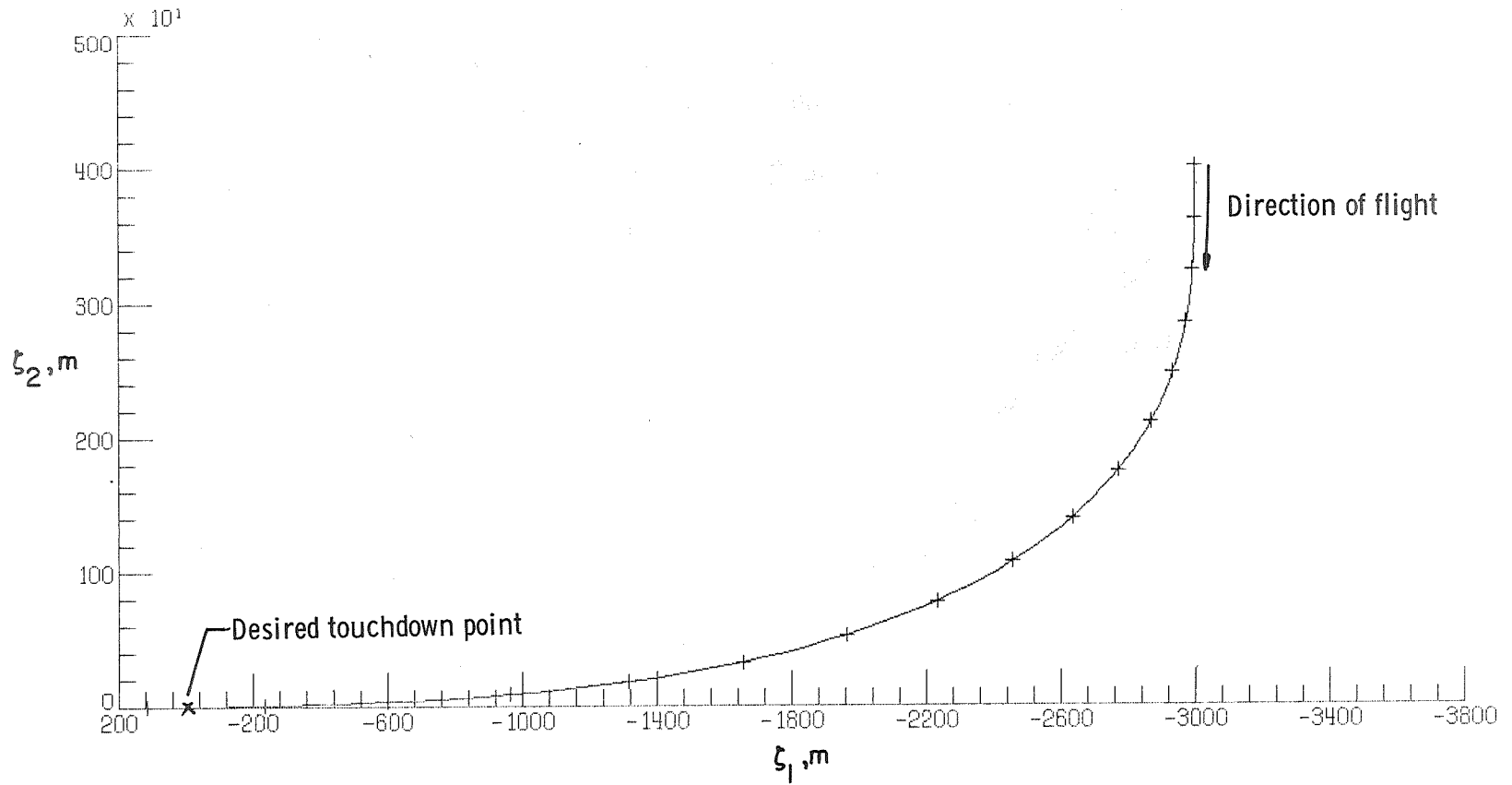
Figure 10.- Ground track for the initial condition $\zeta_1 = -3000$ m, $\zeta_2 = -4000$ m, $H = 540$ m, $\psi_i = -\frac{\pi}{2}$ (case 24 of table II). Tick marks indicate 5-sec intervals.
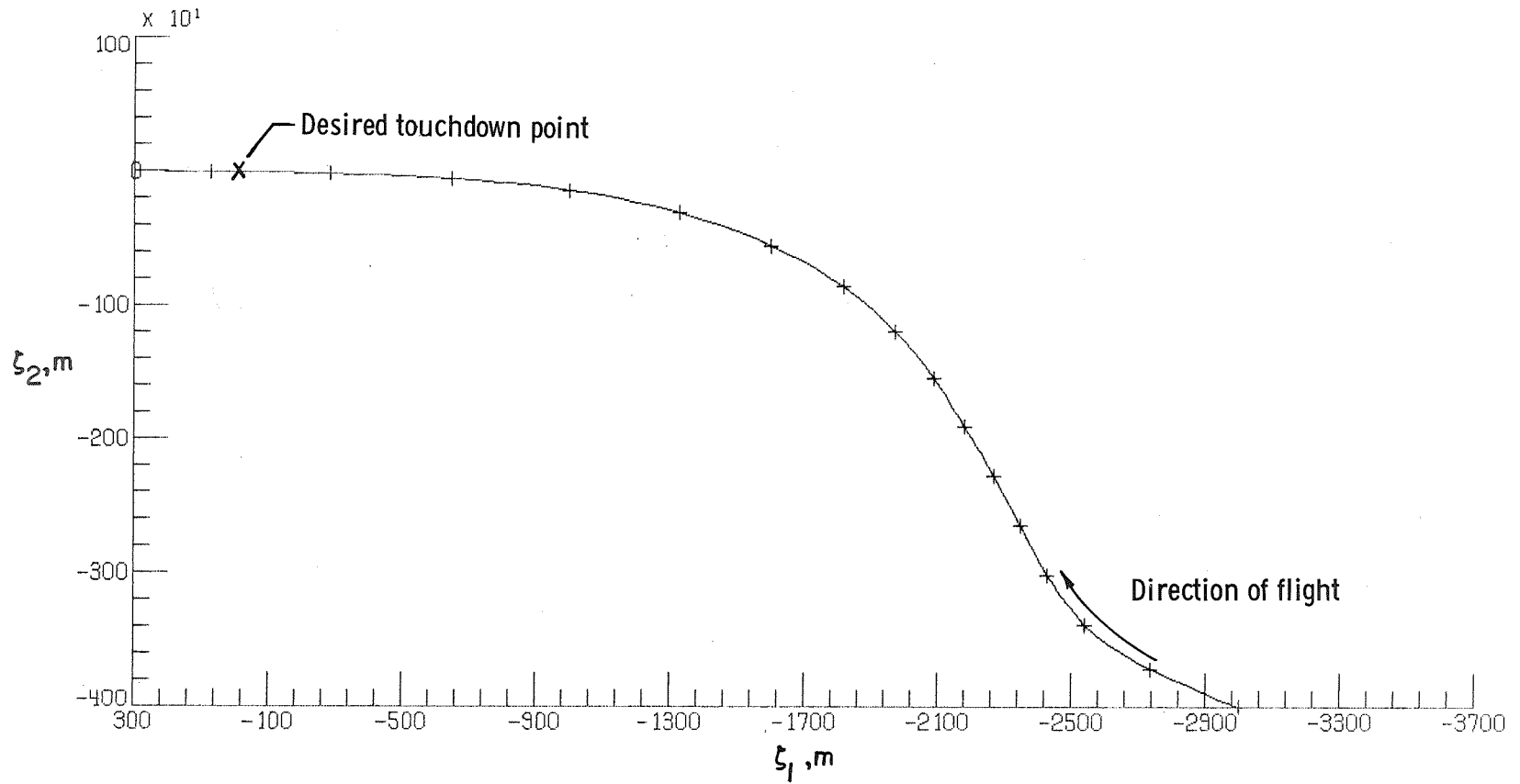
Figure 11.- Ground track for the initial condition ζ_1 = -3000 m, ζ_2 = -4000 m, H = 540 m, $\psi_i = \frac{\pi}{4}$ (case 22 of table II). Tick marks indicate 5-sec intervals.
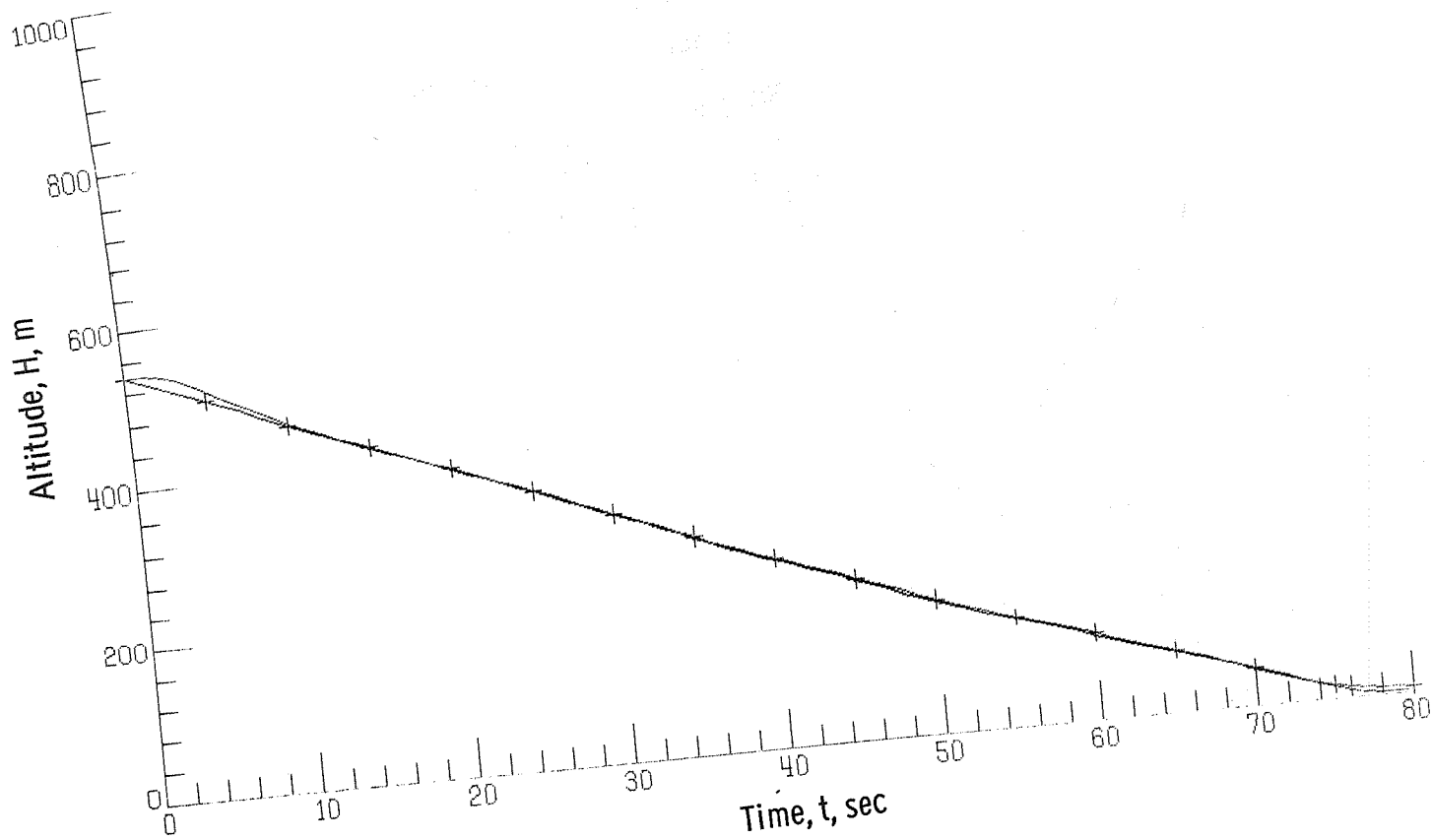
(a)   H = 540 m   (case 21 of table II).

Figure 12.- Altitude tracks for different initial altitudes.
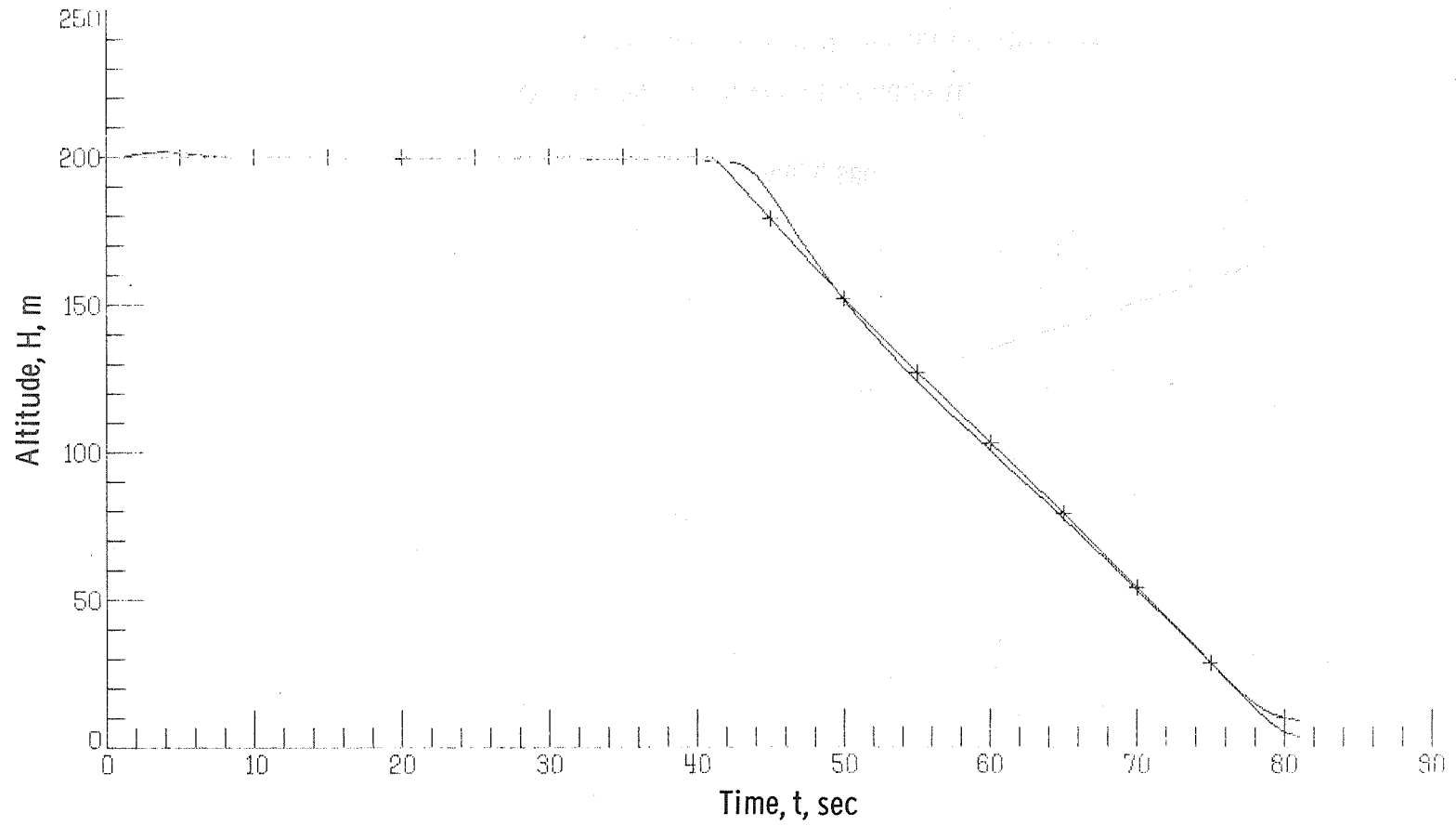
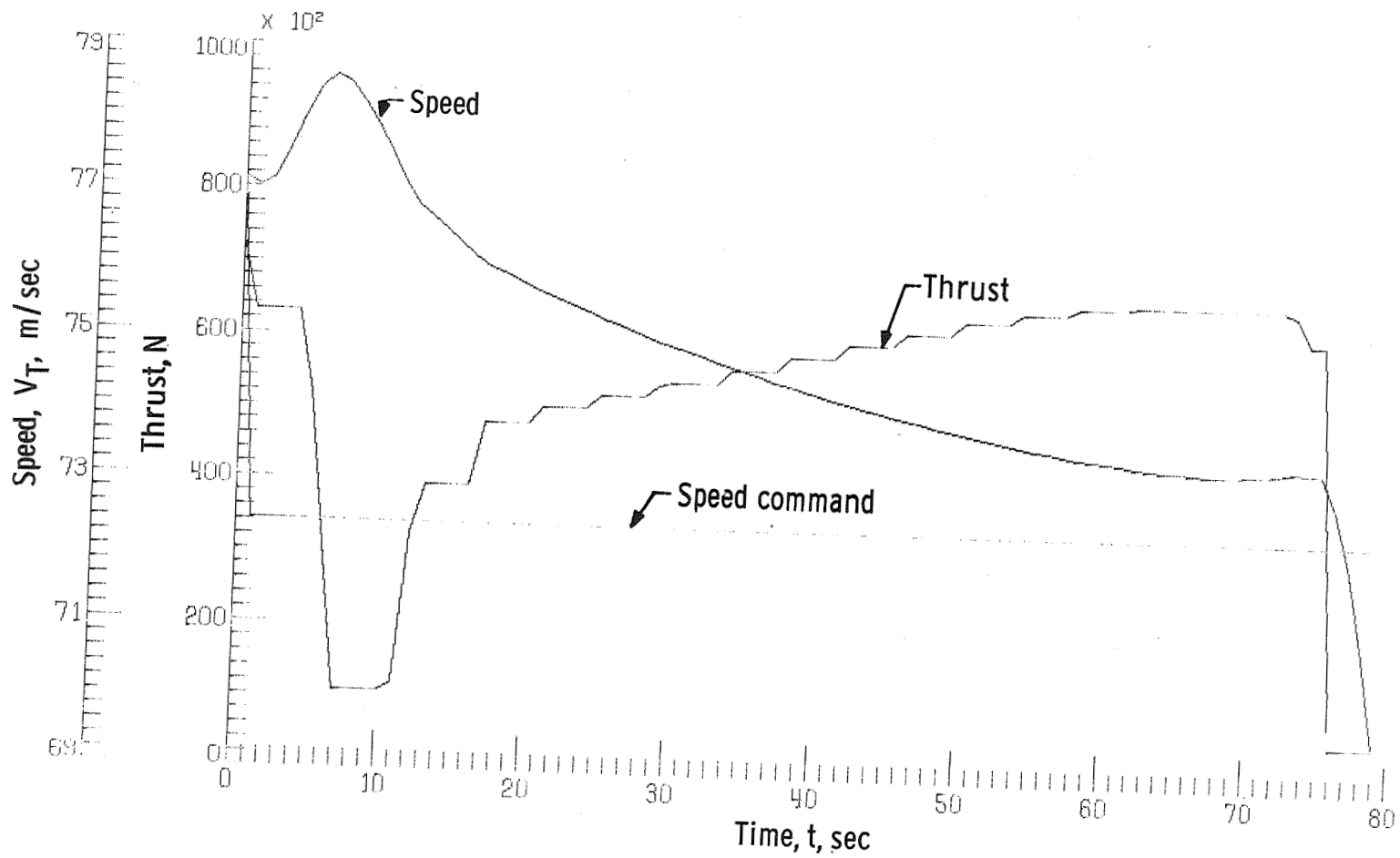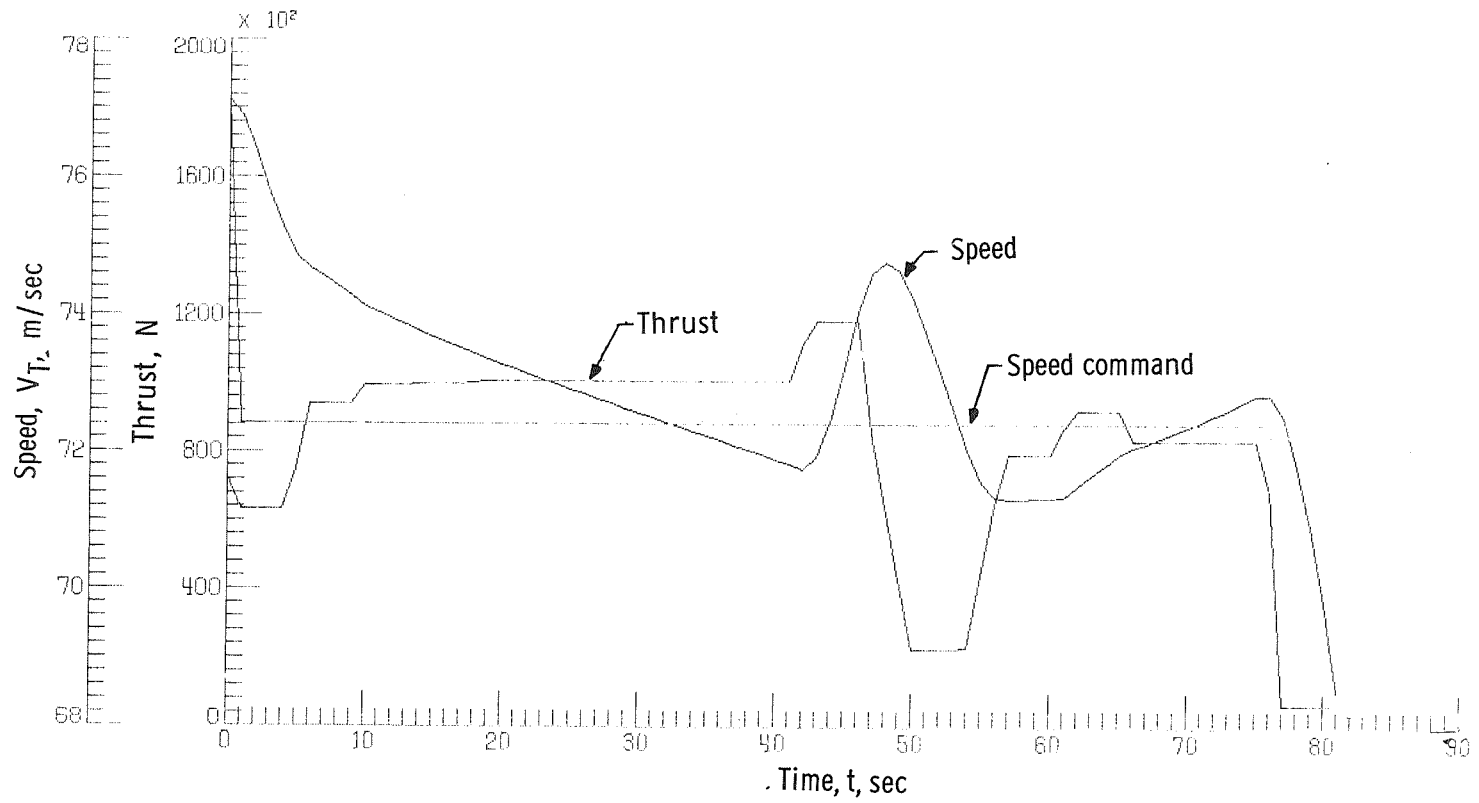(b) H = 200 m (case 28 of table II).

Figure 12.- Concluded.
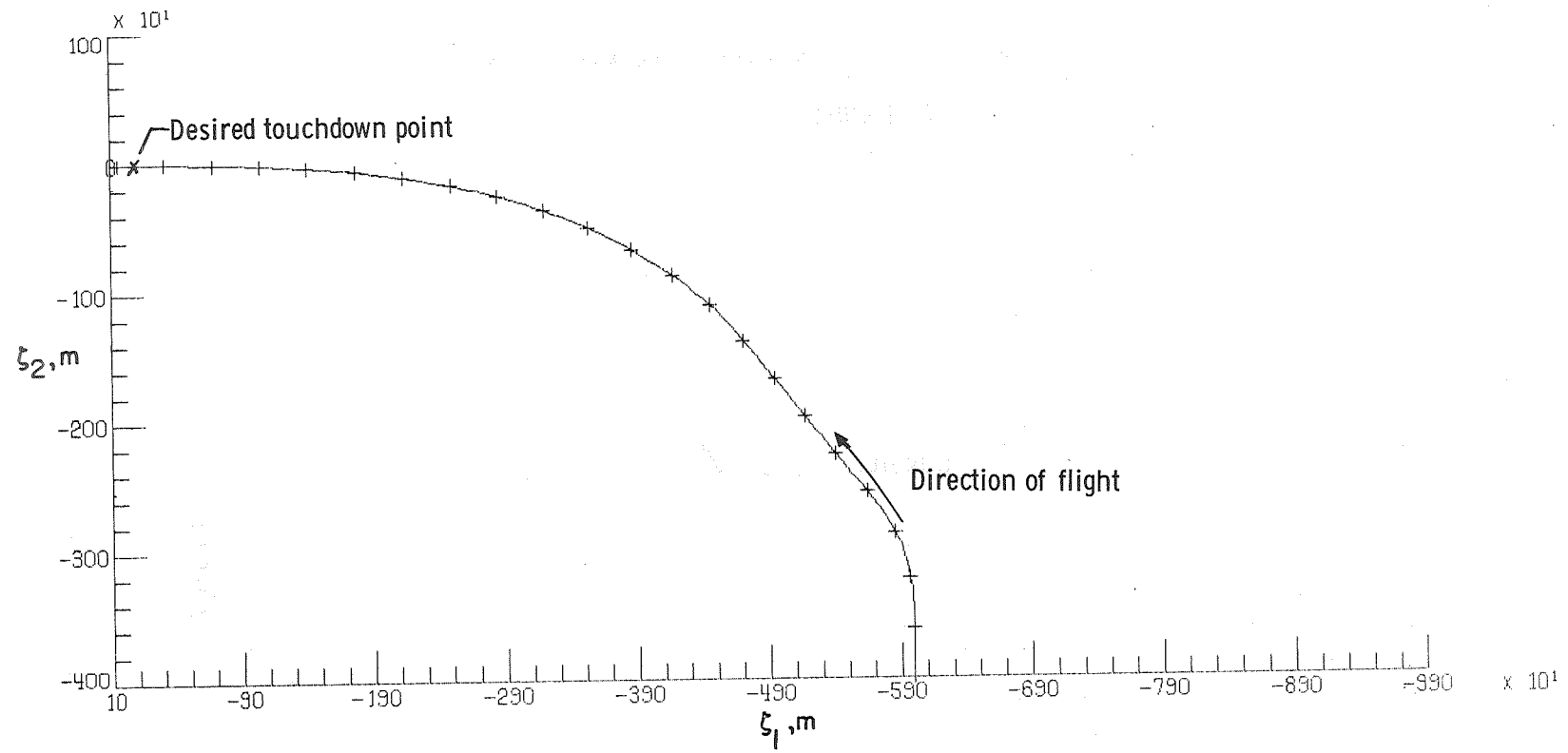
Figure 13.- Basic turn algorithm used with a straight line segment $\zeta_1 = -6000$ m, $\zeta_2 = -4000$ m, H = 540 m, $\psi_i = \frac{\pi}{2}$ (case 31 of table II). Tick marks indicate 5-sec intervals.
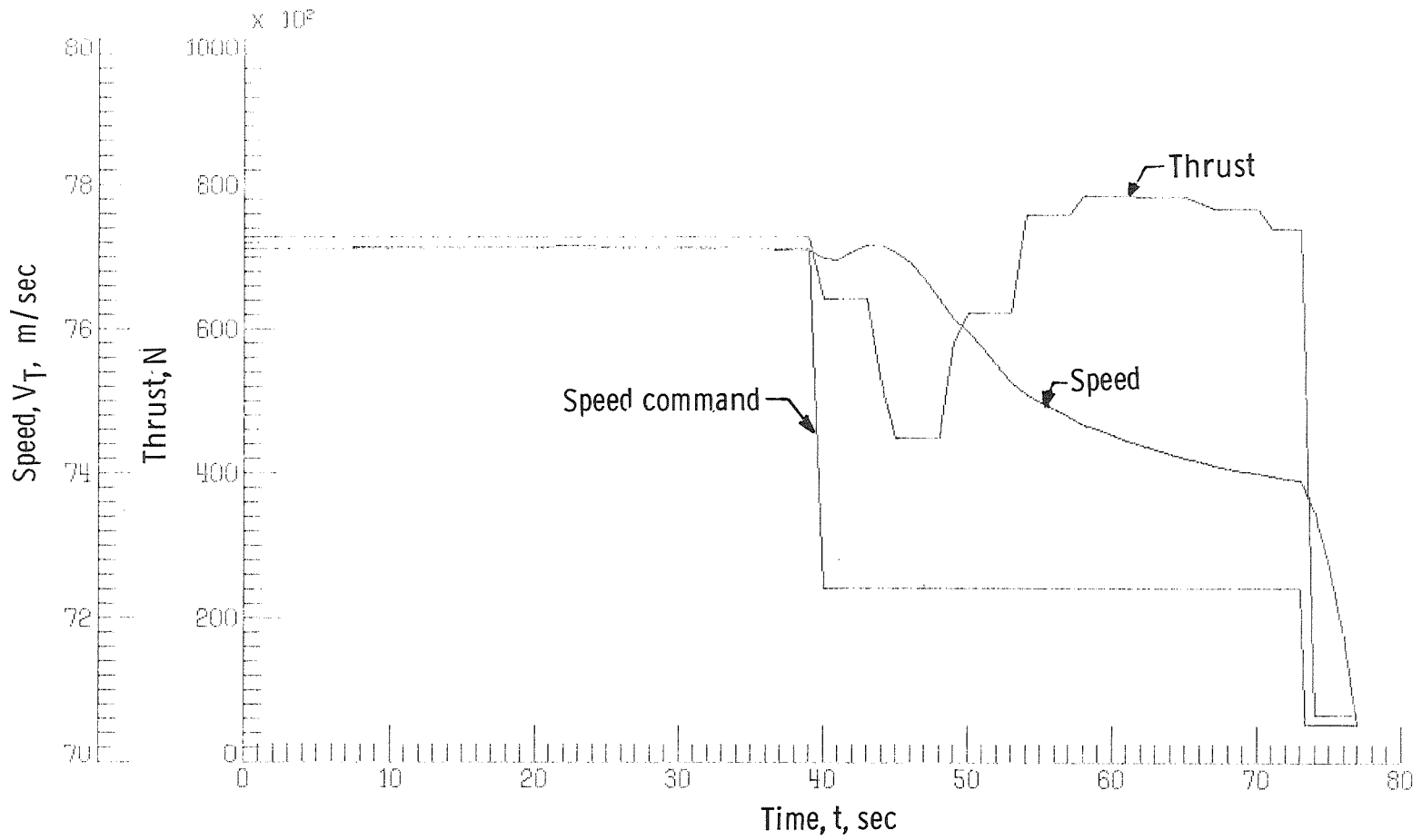
(a) Speed changed and flaps lowered at t = 0 (case 27 of table II).

Figure 14.- Speed and thrust curves.

(b) Constant altitude flight for 39 sec. Speed change and flaps lowered at $t = 0$ (case 28 of table II).

Figure 14.- Continued.

(c) Constant altitude flight for 39 sec.   Flaps lowered with speed change command (case 33 of table II).

Figure 14.- Concluded.

"The aeronautical and space activities of the United States shall be conducted so as to contribute . . . to the expansion of human knowledge of phenomena in the atmosphere and space. The Administration shall provide for the widest practicable and appropriate dissemination of information concerning its activities and the results thereof."
—NATIONAL AERONAUTICS AND SPACE ACT OF 1958

NASA SCIENTIFIC AND TECHNICAL PUBLICATIONS

TECHNICAL REPORTS: Scientific and technical information considered important, complete, and a lasting contribution to existing knowledge.

TECHNICAL NOTES: Information less broad in scope but nevertheless of importance as a contribution to existing knowledge.

TECHNICAL MEMORANDUMS: Information receiving limited distribution because of preliminary data, security classification, or other reasons. Also includes conference proceedings with either limited or unlimited distribution.

CONTRACTOR REPORTS: Scientific and technical information generated under a NASA contract or grant and considered an important contribution to existing knowledge.

TECHNICAL TRANSLATIONS: Information published in a foreign language considered to merit NASA distribution in English.

SPECIAL PUBLICATIONS: Information derived from or of value to NASA activities. Publications include final reports of major projects, monographs, data compilations, handbooks, sourcebooks, and special bibliographies.

TECHNOLOGY UTILIZATION PUBLICATIONS: Information on technology used by NASA that may be of particular interest in commercial and other non-aerospace applications. Publications include Tech Briefs, Technology Utilization Reports and Technology Surveys.

Details on the availability of these publications may be obtained from:
SCIENTIFIC AND TECHNICAL INFORMATION OFFICE
NATIONAL AERONAUTICS AND SPACE ADMINISTRATION
Washington, D.C. 20546